Systems/Circuits

Medial Prefrontal Cortex Innervation of the Basal Forebrain Regulates Behavioral Activation with Prelimbic and Infralimbic Projections Contributing to Distinct Affective Functions in Rats

Mert Genc, Cem Sevinc, Bahar Yuksel, and Gunes Unal
Behavioral Neuroscience Laboratory, Department of Psychology, Boğaziçi University, Istanbul 34342, Turkey

The medial prefrontal cortex (mPFC) regulates affective and motivational behaviors through its projections to subcortical targets, yet the functional contribution of its innervation of the basal forebrain (BF) remains poorly understood. Here, we combined viral tracing, neural activity mapping, molecular characterization, and pathway-specific optogenetic manipulations in adult rats (27 males, 28 females) to investigate the role of prelimbic (PrL) and infralimbic (IL) projections to BF. Using retrograde tracing combined with stress-induced c-Fos mapping, we showed that BF-projecting neurons in both PrL and IL cortices are robustly recruited by acute and chronic stress. Optogenetic activation of these neurons in the BF increased activity, reduced conditioned freezing, and led to real-time place avoidance, indicating a role in behavioral activation and fear suppression. Subregion-specific manipulations of mPFC revealed a functional dissociation. Selective activation of the IL–BF pathway increased activity, suppressed freezing during extinction, and produced place preference. In contrast, activation of the PrL–BF projections produced place avoidance without altering activity levels or conditioned fear responses. Anatomical analysis revealed that BF-projecting mPFC neurons represent a heterogeneous population that may express CaMKIIa as well as different calcium-binding proteins, while some of their axonal terminals in the BF contain VGluT2 or are located in close apposition to PSD95-positive postsynaptic puncta. The majority of the postsynaptic targets were hDlx-expressing inhibitory neurons in the ventral pallidum. Together, these findings identify the BF as a key target in prefrontal control of affective functions, through which PrL and IL projections differentially regulate motivational state, valence processing, and fear memory.

Key words: basal forebrain; behavioral activation; infralimbic; medial prefrontal cortex; prelimbic; ventral pallidum

Significance Statement

The medial prefrontal cortex (mPFC) exerts top–down control over affective behaviors through subcortical projections, with distinct subregions often mediating opposing or complementary functions. We identify the basal forebrain (BF) as a critical mPFC target through which prelimbic (PrL) and infralimbic (IL) glutamatergic projections exert dissociable effects. IL inputs to the BF, which mainly target inhibitory neurons in the ventral pallidum, promote behavioral activation, suppress fear expression, and produce place preference, reflecting positive valence. In contrast, the PrL to BF pathway, which exhibits comparatively sparse innervation, conveys aversive signals and drives behavioral avoidance. These findings reveal a novel circuit mechanism by which medial prefrontal subregions differentially regulate motivational state, valence processing, and fear memory.

Introduction

The medial prefrontal cortex (mPFC) is a key regulator of several limbic functions, including reward-seeking, fear, and anxiety, primarily via its monosynaptic subcortical projections (Room et al., 1985; Hurley et al., 1991; Vertes, 2004; Hänsel and von Känel, 2008; Adhikari et al., 2015; Dixon et al., 2017). Its two subdivisions, the prelimbic (PrL) and the infralimbic (IL) cortices (Gabbott et al., 2003; 2005; Vertes, 2004) play central roles in

Received Jan. 25, 2026; revised July 1, 2026; accepted July 9, 2026.
Author contributions: M.G., C.S., B.Y., and G.U. designed research; M.G., C.S., B.Y., and G.U. performed research; M.G., C.S., B.Y., and G.U. wrote the paper.
This research was funded by grants from EMBO (number, 4432) and the Scientific and Technological Council of Türkiye (number, 325K527) to G.U.
The authors declare no competing financial interests.
Correspondence should be addressed to Gunes Unal at gunes.unal@bogazici.edu.tr.
This paper contains supplemental material available at: https://doi.org/10.1523/JNEUROSCI.0146-26.2026
https://doi.org/10.1523/JNEUROSCI.0146-26.2026

integrating affective processes with autonomic and neuroendocrine systems (Akirav and Maroun, 2007). The PrL sends dense projections to the mediodorsal thalamic nucleus, nucleus accumbens, and basolateral amygdala, through which it modulates goal-directed behavior and stress processing (Sotres-Bayon and Quirk, 2010; Woon et al., 2020; de Kloet et al., 2021; Shih and Chang, 2024). In contrast, the IL projects to the nucleus accumbens, basolateral amygdala, and the bed nucleus of the stria terminalis, contributing to emotion regulation and fear extinction (Sotres-Bayon and Quirk, 2010; Do-Monte et al., 2015; Moorman and Aston-Jones, 2015; Kenwood et al., 2022; Nett et al., 2023). Both mPFC subregions also send significant projections to the basal forebrain (BF; Vertes, 2004; Gabbott et al., 2005), the largest set of neuromodulatory nuclei in the mammalian brain (Zaborszky, 2002). While these projections form part of a cortical–BF–cortical loop that supports BF-driven cortical arousal (Golmayo et al., 2003; Gyengési et al., 2008; Anaclet et al., 2015), the specific affective roles of PrL and IL efferents to the BF remain unknown. Using tract-tracing, neural activation mapping, and optogenetic manipulations combined with postsynaptic target characterization, we identify distinct affective functions of the BF-targeting PrL and IL projections.

The PrL is primarily associated with stress processing and acquired fear expression, mostly via its innervation of the amygdala (Corcoran and Quirk, 2007; Sotres-Bayon and Quirk, 2010; McKlveen et al., 2015). In response to stress, PrL neurons are recruited to mediate active coping responses and to support contextual fear encoding (McKlveen et al., 2015; Rizzo et al., 2017; Johnson et al., 2022). It also sends projections to the BF (Gaykema et al., 1991), which modulates cortical arousal and attentional processing (Hangya et al., 2015; Gielow and Zaborszky, 2017). The IL, in contrast, plays a critical role in the extinction of the conditioned fear (Hartley and Phelps, 2010; Sotres-Bayon and Quirk, 2010). Unlike PrL, IL neurons, which decrease their firing rates during freezing behavior (Giustino et al., 2016), facilitate extinction learning to suppress conditioned fear responses (Vidal-Gonzalez et al., 2006; Sierra-Mercado et al., 2011; Bloodgood et al., 2018; Tao et al., 2021). IL sends particularly dense projections to the BF (Zaborszky et al., 1997; Vertes, 2004), and these BF-targeting neurons increase their firing during extinction learning (Fernandes-Henriques et al., 2025).

BF orchestrates valence processing and behavioral responses to stress, and distinct BF neuronal populations have been implicated in threat-related and aversive behaviors (Johnson et al., 2016; Stephenson-Jones et al., 2020; Moaddab et al., 2021; Maness et al., 2022; Akmese et al., 2023; Hegedüs et al., 2024), making it a candidate region through which PrL and IL inputs may shape affective processing in opposing ways. Anatomical tracing studies have demonstrated that both PrL and IL send topographically organized glutamatergic projections to BF nuclei, including the ventral pallidum (VP), horizontal diagonal band, and substantia innominata (Vertes, 2004; Gabbott et al., 2005).

To understand the specific roles of PrL–BF and IL–BF projection pathways in stress-related behaviors, we used a multilevel approach that combined neural activation mapping with pathway-specific manipulation and neurochemical characterization in male and female Wistar rats. First, we revealed the recruitment of BF-projecting PrL and IL neurons in response to different types of stress. We next tested the functional role of mPFC–BF innervation in affective paradigms using optogenetics. Finally, we selectively activated PrL and IL projections to the BF by axonal stimulation to determine their distinct contributions to locomotor activity, associative conditioning, anxiety-like behavior, social approach-avoidance (SAA), and fear learning.

Materials and Methods

Subjects

A total of 55 experimentally naive adult Wistar rats (3–6 months) were used for three sets of experiments. The stress-induced neural activation experiment/viral tracing included 16 rats ($n = 4$ per group; two males and two females). We used 10 rats (five females and five males) for additional viral tract-tracing and postsynaptic target characterization. The first optogenetics experiment (mPFC–BF activation) involved 5 rats (two males and three females), and the second group of optogenetics experiments was conducted with 24 rats (control, $n = 6$, three females and three males; PrL, $n = 9$, four females and five males; IL, $n = 9$, five females and four males).

All animals were maintained under standardized laboratory conditions (21 ± 1°C; 40–60% relative humidity; 12:12 light/dark cycle) with *ad libitum* access to food and water. Animals in the neural activation experiment were group-housed (four per cage), while animals used for anatomical tracing or optogenetic experiments were housed individually throughout the surgeries and behavioral testing. All procedures were approved by the Boğaziçi University Ethics Committee for the Use of Animals in Experiments.

Stress-induced c-Fos quantification

We investigated the recruitment of the PrL and IL neurons by different types of stress by combining viral tracing and immunohistochemistry for the c-Fos protein. Stereotaxic injections of the AAV9-CaMKIIa-hM4D(Gi)-mCherry (Addgene #50477; volume, 0.5 µl) were targeted to the mPFC (coordinates are given below) to selectively transduce calcium/calmodulin-dependent protein kinase type II subunit alpha (CaMKIIa)-expressing neurons. In parallel, AAVretro-hSyn-Cre-EGFP (Addgene #105540; volume, 0.3 µl) was administered into the BF to enable identification of BF-projecting neuronal populations of the PrL and IL. Sixteen rats were assigned to one of four groups: Control (no stress), Acute Stress (single 90 min restraint before perfusion), Chronic Variable Stress (CVS), or Chronic Restraint Stress (CRS). Both chronic paradigms spanned 10 d; CRS consisted of twice-daily restraint, whereas CVS comprised heterogeneous daily stressors (Kingir et al., 2023). One animal was lost in each chronic stress group during restrainment.

Anatomical analyses were performed on six coronal sections encompassing the mPFC per subject, with each hemisphere treated as an independent data point. Sections containing fewer than 150 $CaMKIIa^+$ cells per mm^2 or fewer than five retrogradely labeled cells per millimeter squared were excluded. The resulting datasets included 28 Control, 27 Acute Stress, 16 CRS, and 19 CVS data points for the PrL and 24 Control, 37 Acute Stress, 23 CRS, and 21 CVS data points for the IL. Data from all experimental groups were pooled for laminar distribution analyses of mPFC–BF projections.

Viral tracing

We carried out two different viral-tracing experiments to reveal and characterize mPFC neurons that project to the BF and to identify the molecular identity of their postsynaptic targets ($n = 4$). One group received bilateral AAV9-mDlx-ChR2-mCherry-Fishell-3 (Addgene #83898; volume, 0.5 µl) injections into the mPFC and AAVretro-hSyn-Cre-EGFP (Addgene #105540; volume, 0.3 µl) into the BF to test for the existence of long-range putative GABAergic mPFC neurons projecting to the BF ($n = 2$). Next, we performed anterograde transsynaptic labeling (Kitanishi et al., 2022) by injecting AAV1-hSyn-Cre-EGFP (Addgene #105540; volume, 0.5 µl) into the mPFC and AAV9-hDlx-GiDREADD-dTomato-Fishell-5 (Addgene #83896; volume, 0.5 µl) into the BF bilaterally ($n = 2$). Since the hDlx enhancer preferentially drives transgene expression in GABAergic neurons (Dimidschstein et al., 2016), this viral combination was used to identify putative GABAergic target neurons in the BF and characterize their molecular profiles using additional immunohistochemistry.

Postsynaptic target characterization

Three target characterization experiments were conducted to identify and characterize BF neurons receiving mPFC input ($n = 6$). In all experiments, we performed anterograde transsynaptic labeling as previously described by injecting AAV1-hSyn-Cre-EGFP (Addgene #105540; volume, 0.4 µl) bilaterally into the mPFC. To determine the neurochemical identity of the postsynaptic target neurons, three separate groups received bilateral BF injections (0.4 µl per hemisphere) of one of the following viruses: AAV9-hDlx-GiDREADD-dTomato-Fishell-5 (Addgene #83896) to label putative GABAergic neurons ($n = 2$), AAV-PHP.eB-BiCHATe27-ChR2-mCherry (Addgene #213830) to label cholinergic neurons (Furlanis et al., 2025; $n = 2$), or AAV9-CaMKIIa-hM3D(Gq)-mCherry (Addgene #50476) to label CaMKIIa$^+$ neurons ($n = 2$).

Optogenetic activation

For the first optogenetic activation experiment, AAV1-hSyn-cre-EGFP (Addgene, #105540; volume, 0.25 µl) and AAV9-EF1a-DIO-hChR2-mCherry (Addgene #35508; volume, 0.25 µl) were stereotaxically delivered into the mPFC, and bilateral optic cannulas were implanted into the BF to enable selective activation of mPFC axon terminals. We examined the projection-specific contributions of BF-projecting neurons within mPFC subregions in a separate experiment. Here, the same viral vectors were injected selectively into either the PrL or IL at a lower volume (0.1 µl), and optic cannulas were implanted into the BF. A control group received only AAV1-hSyn-cre-EGFP (Addgene #105540; volume, 0.25 µl) to mPFC with bilateral optic cannula implanted into the BF.

Fiber-optic cannulas (core diameter, 400 µm; numerical aperture, 0.39) were placed using a cannula holder and secured to the skull with dental adhesive (FGM Ambar Universal) followed by dental cement (FGM Vittra). Both materials were cured using UV light. Optical stimulation was delivered via 465 nm light bilaterally at 40 Hz with 5 ms pulse duration and 40 mW output power at the fiber tip (≈20 mW per hemisphere).

Stereotaxic surgeries

Animals were deeply anesthetized with 4–5% isoflurane induction and placed into a stereotaxic frame (RWD Life Science). Body temperature was kept at ≈36°C via a heating pad, and the anesthesia was maintained with 1–2% isoflurane flow during the procedure. A local anesthetic (10% Vemcaine) was administered both by subcutaneous injection and to the shaved head, followed by the application of povidone-iodine solution before the vertical incision. Injection coordinates were calculated with reference to the bregma point using a rat brain atlas (Paxinos and Watson, 2006) for mPFC (AP, +2.7; ML, ±0.7; DV, −4.0), PrL (AP, +2.7; ML, ±0.7; DV, −3.8), IL (AP, +2.7; ML, ±0.7; DV, −4.8), and BF (AP, 0; ML, ±2.4; DV, −7.9 for viral injections or −7.0 for cannula implantation).

The viral constructs were bilaterally injected (0.1 µl/min rate) with a 1 µl Hamilton syringe using a microinjection pump (Stoelting). Once the injections were completed, the syringes were left in the injection site for 5 min and withdrawn at a rate of 0.1 mm/min to minimize tissue damage and dorsal diffusion. At the end of surgeries with no implants, the incision was sutured; povidone-iodine and local anesthetics (Anestol pomade, 5% lidocaine) were administered to the suture site. Animals were allowed to recover for 3 weeks before behavioral testing.

Behavioral testing

Animals were acclimated to the test room for 5 min prior to each session, and all behavioral tests were video-recorded using a digital camera (Sony HDR-CX625) for subsequent offline analysis. Dependent measures from the open field test (OFT), three-chamber test (TCT), light–dark box (LDB), and SAA were quantified using the EthoVision XT 17 software (Noldus Information Technology). Behavioral data from the real-time place preference (RTPP), conditioned place preference (CPP), and fear conditioning (FC) were analyzed with the ezTrack software (Pennington et al., 2019). All mazes were cleaned with 70% ethanol between sessions to eliminate residual olfactory cues. Behavioral test timelines for each experiment are given in Figures 3*A* and 4*A*.

OFT. A black square arena (70 × 70 × 45 cm) was used for the OFT to assess locomotor activity and anxiety-like behavior (Gencturk and Unal, 2024). In the first optogenetic experiment (mPFC–BF), each OFT session began with a 3 min baseline period preceding optogenetic manipulation. During the first session, animals experienced alternating 3 min epochs with and without optical stimulation. In the second session, following a 3 min baseline period, four cycles of stimulation were applied in 1 min epochs interleaved with 2 min stimulation-free intervals. Similarly, in the second optogenetic experiment, the test began with a 3 min baseline period, followed by four cycles of 1 min stimulation epochs interleaved with 2 min stimulation-free intervals. We quantified both locomotion and general activity in the OFT. Locomotion was defined as the distance traveled, calculated after applying a 2 cm smoothing filter. General activity (duration) encompassed locomotion as well as species-specific movements expressed during static periods, such as rearing, grooming, and major head movements, which were derived from the nonsmoothed data.

TCT. The same arena used for the OFT was modified for the TCT by inserting panels to divide it into three chambers. During the habituation phase, each animal was placed in the maze for 5 min without any social or nonsocial stimuli. Subsequently, two cylindrical cages were positioned in opposite corners of the maze, one containing a same-sex conspecific and the other left empty. The test lasted 15 min and was divided into three 5 min epochs. During the middle epoch, optogenetic stimulation was applied in alternating 30 s light ON/OFF periods throughout the 5 min interval (Leung et al., 2018).

LDB. The LDB apparatus (41 × 43 × 31 cm) consisted of two equal compartments separated by a partition and a door along the 43 cm side. The dark chamber (0 lx) was constructed with opaque walls and a cover, whereas the light chamber (≈200 lx) had transparent acrylic walls and remained uncovered. In the mPFC–BF experiment, each session began with a 3 min baseline period, followed by two alternating 3 min epochs with and without optogenetic stimulation. In the second set of optogenetic experiments, the sessions consisted of a 3 min baseline period, four sets of epochs consisting of 2 min without stimulation followed by a 1 min stimulation period, and a final 2 min no-stimulation period.

SAA. The SAA was conducted in the same black square arena (70 × 70 × 45 cm) used for the OFT, to minimize novelty stress. During the habituation phase, each animal was placed in the maze for 1 min without any social or nonsocial objects. Subsequently, an empty cylindrical cage was placed at one edge of the maze for 5 min. Optogenetic stimulation was delivered in five alternating 1 min off and 1 min on epochs during this period. The empty cage was then replaced with one containing a same-sex conspecific and reintroduced into the maze for an additional 5 min, with optogenetic stimulation delivered in the same alternating manner.

FC and extinction. We employed a modified 3 d pavlovian FC paradigm (Totty et al., 2023), which included contextual and cued extinction sessions following conditioned stimulus (CS)–unconditioned stimulus (US) pairings. Fear acquisition took place in a chamber (Context A; 21 × 45 × 27 cm) with transparent gray acrylic walls and ceiling and a grid floor composed of 32 metal rods for footshock delivery. Animals were allowed 3 min to explore the chamber to record their baseline activity, after which five CS–US pairings were administered. The CS consisted of a 10 s auditory tone (8 kHz, 80 dB), coterminating with the US, a 2 s footshock (1.0 mA). Intertrial intervals (ITIs) were pseudorandomized between 50 and 70 s.

Contextual extinction was conducted the following day in the same apparatus as the acquisition phase, maintaining identical contextual features. Each session began with a 2 min baseline period, followed by alternating 1 min epochs with optogenetic stimulation and 2 min epochs without stimulation, repeated for a total of 10 cycles.

On the third day, cued extinction was performed in a distinct chamber (Context B; 41 × 43 × 31 cm) with a black opaque floor and transparent walls located in a different part of the test room. To ensure contextual

novelty, the chamber was cleaned with 70% ethanol and then wiped with 1% peppermint oil to provide an olfactory cue. Cued extinction consisted of a 3 min baseline period, followed by 44 CS presentations delivered with fixed 30 s, and concluded with a 1 min no-stimulation period following the final CS. Optogenetic stimulation was delivered exclusively during CS presentations. Animals first received four CS presentations without stimulation, followed by four CS presentations with stimulation, and this sequence was repeated five times.

To measure spontaneous recovery, we conducted a second cued extinction session 10 d after the first cued extinction experiment. This session consisted of a 3 min baseline period, followed by 20 CS presentations delivered with fixed 30 s ITIs, and concluded with a 1 min no-stimulation period following the final CS. Optogenetic stimulation parameters (stimulation only during CS presentations, four ON and four OFF epochs) were the same as the first cued extinction session.

RTPP. The RTPP test was done in a three-compartment apparatus ($34 \times 15 \times 40$ cm) consisting of two equal compartments connected by a central neutral zone ($10 \times 15 \times 40$ cm). At the start of each session, animals were placed in the neutral zone for 1 min with the connecting doors closed. The doors were then opened, allowing free exploration of the apparatus for 20 min. During the first 10 min, one compartment was designated as the stimulation-paired side, where animals received continuous optogenetic stimulation whenever they entered and remained within that zone. After 10 min, the stimulation-paired side was switched to the opposite compartment using the same contingency. The identity of the stimulation-paired side was counterbalanced across subjects to control for potential chamber bias. The amount of time spent in each chamber was scored via automated video tracking.

CPP. CPP was evaluated using the same three-compartment RTPP apparatus. The procedure was conducted over 2 consecutive days. On Day 1 (pretest and conditioning), animals first underwent a 10 min pretest. They were confined to the neutral zone for 15 s, after which the doors were opened, and free exploration of all compartments was permitted. Conditioning followed, with counterbalanced assignment of the stimulation-paired chamber. Each animal was confined to the stimulation-paired side for 7.5 min, during which continuous optogenetic stimulation was delivered. After all animals completed this phase, they were confined to the nonstimulation side for 7.5 min with optic cables attached but without stimulation. This conditioning cycle was repeated twice. On Day 2 (test session), animals were evaluated without the optic cables attached. Each trial began with a 15 s confinement in the neutral zone, followed by 15 min of unrestricted access to all compartments. The amount of time spent in each chamber was scored via automated video tracking.

Tissue preparation and immunohistochemistry

Animals were deeply anesthetized with a terminal intraperitoneal injection of ketamine (100 mg/kg) and xylazine (10 mg/kg), followed by transcardial perfusion with 0.9% saline and subsequently 4% depolymerized paraformaldehyde (PFA) in phosphate-buffered saline (PBS). Brains were removed, post-fixed in PFA for two nights at 4°C, rinsed in PBS (3×10 min), and stored in PBS containing 0.05% sodium azide. Coronal sections (50 µm thickness) were obtained using a vibratome (VT1000S, Leica Biosystems) and maintained in PBS-azide until further processing.

For immunohistochemistry, free-floating sections were first washed in 0.3% PBS with Triton X-100 (PBS-Tx; 3×10 min) to facilitate antibody penetration, followed by 1 h blocking at room temperature in normal horse or goat serum. Sections were then incubated with primary antibodies (Table 1) for 48–72 h at 4°C. Following primary incubation, slices were rinsed in PBS-Tx (3×10 min) and subsequently incubated with the following secondary antibodies for 4 h at room temperature: goat anti-rabbit IgG (H + L) Alexa Fluor 405 (Invitrogen Antibodies catalog #A-31556, RRID: AB221605; 1:500), donkey anti-rabbit IgG (H + L) Alexa Fluor Plus 405 (Invitrogen Antibodies catalog #A48258, RRID: AB2890547; 1:500), donkey anti-guinea pig IgG (H + L) Alexa Fluor 647 (Jackson ImmunoResearch Laboratories catalog #706-605-148, RRID: AB2340476; 1:500), donkey anti-mouse IgG (H + L) Alexa Fluor 647 (Jackson ImmunoResearch Laboratories catalog #715-605-150, RRID: AB2340862; 1:500), and donkey anti-rabbit IgG (H + L) Alexa Fluor 647 (Jackson ImmunoResearch Laboratories catalog #711-605-152, RRID: AB2492288; 1:500). After final washes, sections were mounted onto glass slides and coverslipped using Fluoromount (Thermo Fisher Scientific catalog #00-4958-02) for long-term preservation and fluorescence imaging.

Table 1. Primary antibodies

Molecule	Host species	Dilution	Source, catalog #	Immunogen
CB	Rabbit	1:1,000	Swant, CB38	Recombinant rat CB D-28k
PV	Rabbit	1:1,000	Abcam, AB11427	Native full-length protein corresponding to rat PV
SCGN	Guinea pig	1:1,000	Synaptic Systems, 436004	Recombinant protein corresponding to AA 1–276 from mouse SCGN
c-Fos	Guinea pig	1:5,000	Synaptic Systems, 226 308	Synthetic peptide corresponding to residues near the amino terminus of rat c-Fos
Gephyrin	Guinea pig	1:250	Synaptic Systems, 147 004	Recombinant protein corresponding to AA 326–768 from rat gephyrin
VGluT2	Guinea pig	1:250	Synaptic Systems, 135 404	Synthetic peptide corresponding to residues near the carboxy terminus of rat VGluT2
PSD95	Mouse	1:250	Synaptic Systems, 124 011	Recombinant protein corresponding to PDZ-domain of mouse PSD95
Leu-enkephalin	Rabbit	1:1,000	Abcam, AB8902	Synthetic peptide within rat leu-enkephalin

Microscopy and cell counting

Epifluorescence imaging was performed using an Olympus BX43 microscope equipped with a monochrome CCD camera (Olympus XM10) and controlled via the Olympus cellSens Imaging Software v2.2. Images were acquired with 4× (Plan Apochromat, NA 0.2, Nikon), 10× (Plan Fluor, NA 0.3, Nikon), and 20× (Plan Fluor, NA 0.5, Nikon) objectives. Fluorescence detection was carried out using four filter sets optimized for DAPI, Alexa Fluor 488, Cy3, and Cy5, enabling visualization of Alexa Fluor 405, Alexa Fluor 488/EGFP, mCherry/dTomato, and Alexa Fluor 647 signals.

Confocal imaging was conducted with a Leica SP8 microscope (Leica Microsystems) using the LAS X software at a minimum resolution of $1,024 \times 1,024$ pixels. We used 10× Plan Fluotar (NA 0.3, dry), 20× Plan Fluotar (NA 0.4, dry), or 40× Plan Apochromat objectives (NA 1.10, water immersion). Excitation was provided by 405, 488, 552, and 638 nm lasers, and emitted signals were detected using PMT detectors. The confocal pinhole was adjusted to 1 Airy unit. *Z*-stacks were acquired with a step size corresponding to half the optical section thickness. Uniform adjustments of brightness and contrast were applied across entire images using the FIJI distribution of ImageJ (Schindelin et al., 2012), without nonlinear processing or selective modifications.

Labeled neurons were automatically segmented and quantified in the BF or in coronal sections spanning +3.10 to +2.70 mm relative to bregma point, encompassing the IL and PrL cortices (Paxinos and Watson, 2006). Confocal images were cropped with FIJI (ImageJ), and automatic cell segmentation was performed with CellPose (Stringer et al., 2021), using consistent threshold and cell diameter parameters across all images. A custom Python script was then used to quantify spatial distributions in manually cropped images. For laminar distribution analyses, the script virtually divided the images into 10 µm bins between the midline (cortical surface, superficial Layer 1) and deep Layer 6, calculating the number of labeled cells within each bin. Colocalization of fluorophores and markers was assessed using segmentation masks and intercellular distances, with a threshold of 3 pixels applied to classify overlapping

cells. The script also automatically computed the bin areas, enabling density measurements for both total and overlapping cells across all bins.

For histological analyses, a single image was acquired from each hemisphere of every coronal section, ensuring that sampling areas did not overlap. Labeled cells were quantified independently in each image. Accordingly, each histological data point corresponds to the quantification obtained from one hemisphere of a single section. For each data point, animal identity, rostrocaudal section level, hemisphere, and experimental group were recorded. The numbers of animals, sections, and histological data points included in each analysis are reported in the corresponding Results sections.

Statistical analysis

All statistical analyses were performed using standard parametric methods after verifying that data met assumptions of normality and homogeneity of variance. Group comparisons involving more than two conditions were analyzed using one-way or two-way ANOVAs, including repeated-measures ANOVAs where appropriate, followed by Tukey's HSD post hoc tests for multiple comparisons. Paired or unpaired two-tailed *t* tests were used for direct comparisons between two conditions, as specified. Effect sizes are reported as η^2 for ANOVAs and were calculated for *t* tests where relevant. For behavioral time-course analyses, repeated-measures designs were applied to account for within-subject factors. Correlational analyses were conducted using Pearson's correlation coefficient to assess relationships between stimulation-induced changes in locomotor activity and freezing behavior. Data are reported as mean ± SEM unless otherwise stated, and statistical significance was set at $p < 0.05$ for all analyses. All figures and statistical analyses were generated using GraphPad Prism (v9.3).

Results

Viral tracing combined with stress-induced neuronal activation in the mPFC

AAVretro-hSyn-Cre-EGFP injections into the BF covered the ventral pallidum, substantia innominata, horizontal diagonal band, and magnocellular nucleus and led to many retrogradely labeled neurons in both the PrL and IL (Fig. 1*A*). The density of mPFC projections to the BF was significantly higher in the IL compared with the PrL ($t_{(192)} = 2.645$; $p = 0.0088$; 95% CI = [6.00, 41.20]; $\eta^2 = 0.036$, unpaired *t* test). Projection profiles showed that PrL projections peaked (≈200 cells/mm^2) at ∼650 µm from the midline, whereas IL projections exhibited peak density (≈300 cells/mm^2) ∼500 µm, revealing a topographical difference (Fig. 1*B*). Consistent with the previous reports (Fernandes-Henriques et al., 2025), the largest portion of mPFC–BF projections originated from Layer 5 in both IL and PrL, with relatively fewer projection neurons observed in Layers 2/3 and 6.

PrL cortex

The density of c-Fos-immunopositive (+) cells in the PrL differed significantly between groups ($F_{(3,85)} = 36.66$; $p < 0.0001$; $\eta^2 = 0.5641$; one-way ANOVA; Fig. 1*C*,*D*). Control animals showed lower densities compared with Acute ($p < 0.0001$; 95% CI [−520.6, −304.6]), CRS ($p < 0.0001$; 95% CI [−374.5, −136.8]), and CVS ($p < 0.0001$; 95% CI [−464.5, −214.1]) groups. The Acute Stress group also exhibited higher density than CRS ($p = 0.0046$; 95% CI [38.1, 275.8]), whereas differences between Acute and CVS ($p = 0.4223$; 95% CI [−51.9, 198.5]), as well as CRS and CVS ($p = 0.3683$; 95% CI [−218.3, 50.9]) groups, were not significant (Fig. 1*D*, left). Consistent with these findings, density plots revealed that while control animals had a subtle peak in c-Fos–expressing cells in Layer 3 (≈400 cells/mm^2), Acute Stress produced the strongest peak (≈1,200 cells/mm^2 at ≈500 µm from the midline), followed by CVS (≈1,100 cells/mm^2, sustained between 500 and 800 µm) and CRS groups (≈800 cells/mm^2 near 600 µm; Fig. 1*C*).

The overall density of CaMKIIa-labeled neurons in the PrL did not differ between groups ($F_{(3,85)} = 1.341$; $p = 0.2667$; $\eta^2 = 0.0452$, one-way ANOVA), nor did the density of retrogradely labeled BF-projecting neurons ($F_{(3,85)} = 1.684$; $p = 0.1766$; $\eta^2 = 0.0561$), indicating that baseline labeling was comparable across conditions. In contrast, c-Fos expression within CaMKIIa-expressing neurons differed significantly among groups ($F_{(3,85)} = 12.81$; $p < 0.0001$; $\eta^2 = 0.3114$, one-way ANOVA). Control animals exhibited significantly fewer c-Fos + CaMKIIa neurons than Acute ($p < 0.0001$; 95% CI [−6.65, −2.03]), CRS ($p = 0.0006$; 95% CI [−6.47, −1.39]), and CVS ($p < 0.0001$; 95% CI [−8.13, −2.78]) groups. No differences were observed among the stress-exposed groups (Acute vs CRS, $p = 0.9734$; Acute vs CVS, $p = 0.6974$; CRS vs CVS, $p = 0.5088$; Fig. 1*D*, center).

Similarly, c-Fos expression in retrogradely labeled mPFC–BF projection neurons differed significantly between groups ($F_{(3,85)} = 10.37$; $p < 0.0001$; $\eta^2 = 0.268$, one-way ANOVA), with the Control group exhibiting significantly lower percentages compared with Acute ($p < 0.0001$; 95% CI [−14.24, −4.52]), CRS ($p = 0.0005$; 95% CI [−13.77, −3.07]), and CVS groups ($p = 0.0026$; 95% CI [−13.47, −2.20]), which were comparable (Acute vs CRS, $p = 0.9659$; Acute vs CVS, $p = 0.8902$; CRS vs CVS, $p = 0.9942$; Fig. 1*D*, right).

IL cortex

The density of c-Fos–positive cells in the IL also differed between groups ($F_{(3,101)} = 46.45$; $p < 0.0001$; $\eta^2 = 0.5798$, one-way ANOVA), with the Control group showing significantly lower density of c-Fos–expressing cells compared with Acute ($p < 0.0001$; 95% CI [−379.0, −241.0]), CRS ($p < 0.0001$; 95% CI [−285.1, −131.4]), and CVS groups ($p < 0.0001$; 95% CI [−297.5, −140.1]; Fig. 1*E*,*F*). The Acute Stress group also exhibited significantly higher density of c-Fos expression relative to both CRS ($p = 0.0014$; 95% CI [31.8, 171.6]) and CVS ($p = 0.0070$; 95% CI [19.3, 163.2]), whereas CRS and CVS did not differ significantly ($p = 0.9859$; 95% CI [−89.97, 69.01]; Fig. 1*F*, left). Control animals exhibited the lowest neural activation overall, with values not exceeding ≈250 cells/mm^2. Acute Stress induced the strongest response, peaking around ≈850 cells/mm^2 at ≈500 µm from the midline. CVS animals displayed elevated density (≈650 cells/mm^2) with a broad distribution spanning ≈500–800 µm, whereas CRS animals showed an intermediate peak (≈550 cells/mm^2) near 600 µm (Fig. 1*E*).

Analysis of c-Fos expression within IL CaMKIIa neurons revealed a significant group effect ($F_{(3,101)} = 14.26$; $p < 0.0001$; $\eta^2 = 0.2976$, one-way ANOVA). The Control group exhibited significantly fewer c-Fos + CaMKIIa neurons compared with Acute ($p < 0.0001$; 95% CI [−6.03, −2.44]), CRS ($p = 0.0022$; 95% CI [−4.80, −0.80]), and CVS ($p < 0.0001$; 95% CI [−6.05, −1.96]) groups, while no differences were observed among the stress-exposed groups (Acute vs CRS, $p = 0.1714$; Acute vs CVS, $p = 0.9879$; CRS vs CVS, $p = 0.4284$; Fig. 1*F*, center).

Analysis of c-Fos expression in retrogradely labeled IL–BF neurons also revealed a significant group effect ($F_{(3,101)} = 5.115$; $p = 0.0025$; $\eta^2 = 0.1319$, one-way ANOVA). Within the BF-projecting IL population, the control group exhibited significantly fewer c-Fos$^+$ retrogradely labeled neurons compared with the Acute ($p = 0.0081$; 95% CI [−8.69, −0.96]), CRS ($p = 0.0055$; 95% CI [−9.88, −1.28]), and CVS groups ($p = 0.0181$; 95% CI [−9.45, −0.64]). No significant differences were observed among the stress-exposed groups (Acute vs CRS, $p = 0.9587$; Acute vs CVS, $p = 0.9990$; CRS vs CVS, $p = 0.9893$; Fig. 1*F*, right).

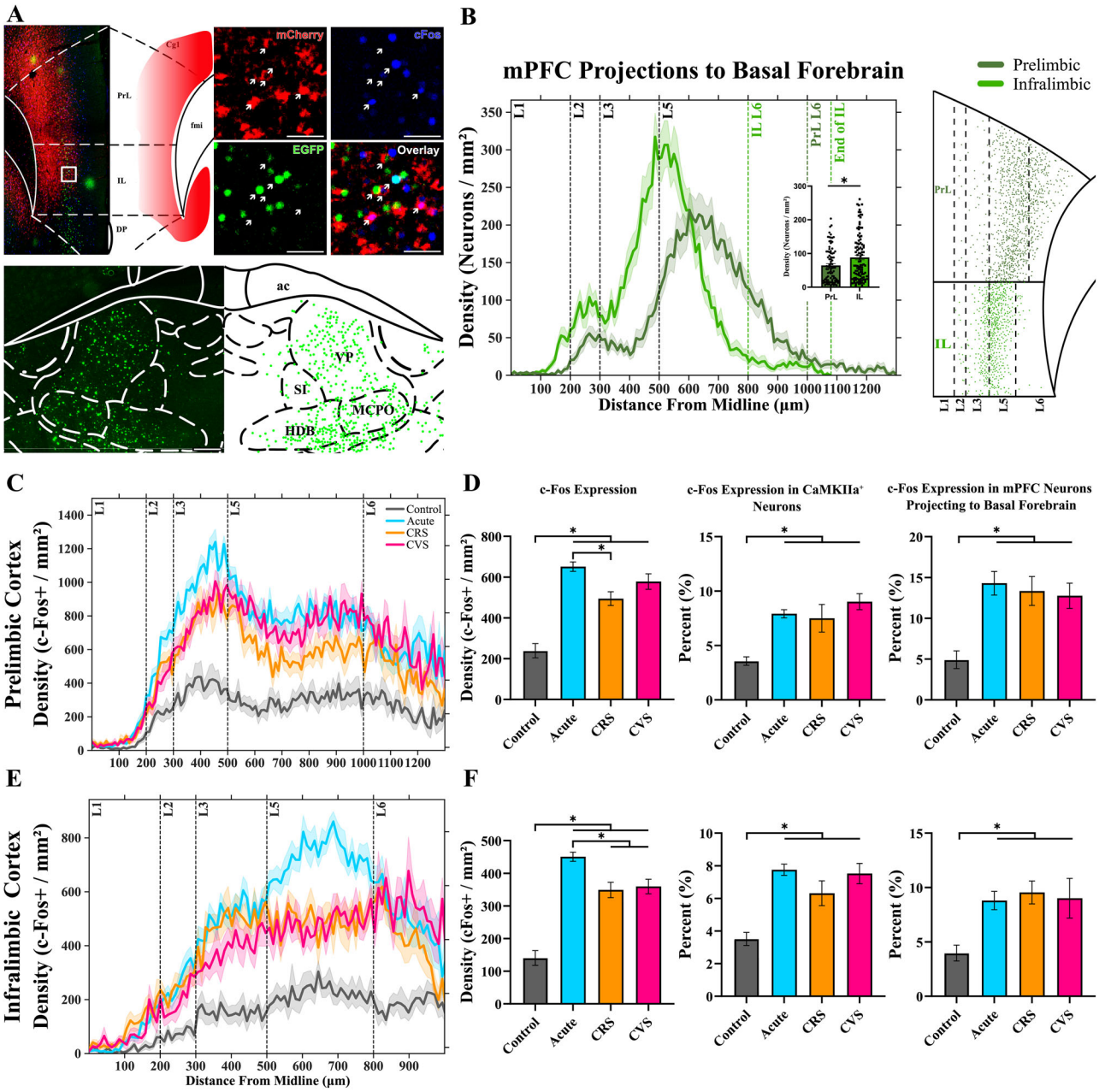

Figure 1. Quantitative analysis of c-Fos$^+$, CaMKIIa$^+$, and retrogradely labeled neurons in the mPFC. ***A***, Schematics and representative images of AAV9-CaMKIIa-hM4D(Gi)-mCherry injections into the mPFC and AAVretro-hSyn-Cre-EGFP injections into the BF (scale bars, 200 µm). High-magnification images show overlays of c-Fos$^+$ and retrogradely labeled neurons (scale bars, 50 µm). ***B***, Distribution of retrogradely labeled cells in mPFC and a representative schematic made from three consecutive 50 µm sections from one animal. ***C***, ***E***, Distribution of c-Fos$^+$ cells in the PrL (***C***) and IL (***E***) cortical layers across control and stress groups. ***D***, ***F***, Quantification of c-Fos$^+$ cell density and the percentage of these cells within CaMKIIa$^+$ and retrogradely labeled neuronal populations in the PrL (***D***) and IL (***F***). Error bars depict SEM. *$p < 0.05$. Abbreviations: DP, dorsal peduncular; fmi, forceps minor of the corpus callosum; SI, substantia innominata; VP, ventral pallidum; ac, anterior commissure; HDB, horizontal limb of the diagonal band of Broca; MCPO, magnocellular nucleus; CRS, chronic restrain stress; CVS, chronic variable stress.

Optogenetic activation of the mPFC–BF projections

Validation of virus injections and transsynaptic labeling in the BF

The AAV1-hSyn-Cre-EGFP (Addgene #105540; volume, 0.5 µl) virus used for Cre expression labeled both the mPFC neurons at the injection site (Fig. 2*A*) and their postsynaptic targets (Fig. 2*E–K*), consistent with previous reports (Kitanishi et al., 2022). In addition, the Cre-dependent virus driving ChR2 expression robustly labeled the axons of Cre-expressing mPFC neurons (Fig. 2*B*,*C*). To verify the placement of the optic cannula, we examined the implantation site and observed a dense population of mPFC-derived axons coursing through the internal capsule and projecting ventrally into the ventral pallidum (Fig. 2*D*,*E*). We also detected postsynaptic EGFP-positive neurons in the diagonal band of Broca. Finally, high-magnification confocal imaging confirmed that axons originating from mPFC neurons closely appose the labeled postsynaptic neurons in the BF (Fig. 2*F–K*).

OFT Day 1

Total distance traveled in the OFT across stimulation epochs revealed a significant main effect of time with a trend toward increased locomotor activity during stimulation periods ($F_{(14,56)} = 4.751$; $p < 0.0001$; $\eta^2 = 0.5429$, repeated-measures ANOVA; Fig. 3*B*, left). The animals traveled significantly greater

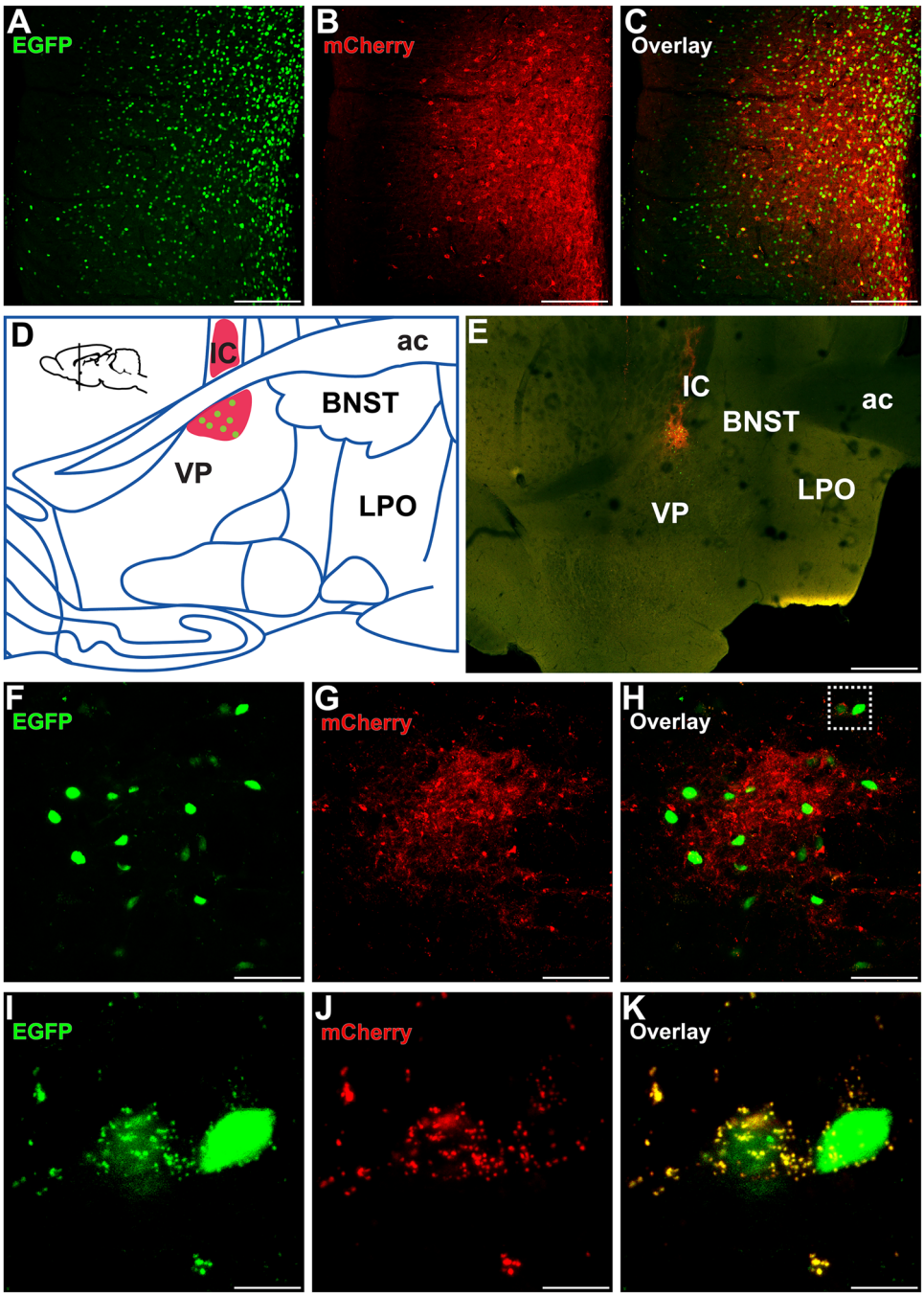

Figure 2. Verification of the viral strategy for selective activation of mPFC projections to the BF. ***A***, EGFP-expressing neurons in the IL following AAV1-hSyn-Cre-EGFP injection into the mPFC. ***B***, Cre-dependent expression of ChR2-mCherry. ***C***, Overlay image (scale bars, 200 µm). ***D***, Schematic illustration of the projection pathway from the mPFC to the BF. ***E***, Low-magnification image showing dense mPFC-derived axons coursing through the internal capsule (IC), passing the anterior commissure (ac), and terminating in the ventral pallidum (VP; scale bar, 500 µm). ***F–H***, High power confocal images showing EGFP-expressing postsynaptic neurons in the BF and dense mPFC-derived mCherry^{+} axons surrounding them. Overlay image shows close apposition of presynaptic axons and postsynaptic neurons (scale bars, 50 µm). ***I–K***, High-magnification images of the boxed region in ***H*** (scale bars, 10 µm).

distances during light ON periods compared with light OFF periods ($t_{(4)} = 3.728$; $p = 0.0203$; 95% CI [25.01, 171.0]; $\eta^2 = 0.7765$, paired *t* test; Fig. 3*B*, right).

Rearing behavior also increased during stimulation, with animals displaying significantly more rearing events during ON compared with OFF periods ($t_{(4)} = 5.281$; $p = 0.0062$; 95% CI [1.302, 5.798]; $\eta^2 = 0.8746$, paired *t* test). In contrast, analysis of time spent in the center of the open field, a measure of anxiolytic response, revealed no effect of stimulation ($t_{(4)} = 1.567$; $p = 0.1921$; 95% CI [−2.13, 7.66]; $\eta^2 = 0.3805$, paired *t* test).

OFT Day 2

Locomotor activity in the second OFT session also showed a significant main effect of time ($F_{(14,56)} = 6.032$; $p < 0.0001$; $\eta^2 = 0.60$, one-way repeated–measures ANOVA; Fig. 3*C*, left), with the time-course data indicating a consistent increase in travel distance during stimulation periods relative to light OFF periods. In addition, locomotor activity across prestimulation, stimulation, and poststimulation epochs revealed a main effect of condition ($F_{(2,8)} = 32.37$; $p = 0.0001$; $\eta^2 = 0.89$; Fig. 3*C*, right). Locomotor activity of the animals was significantly higher during

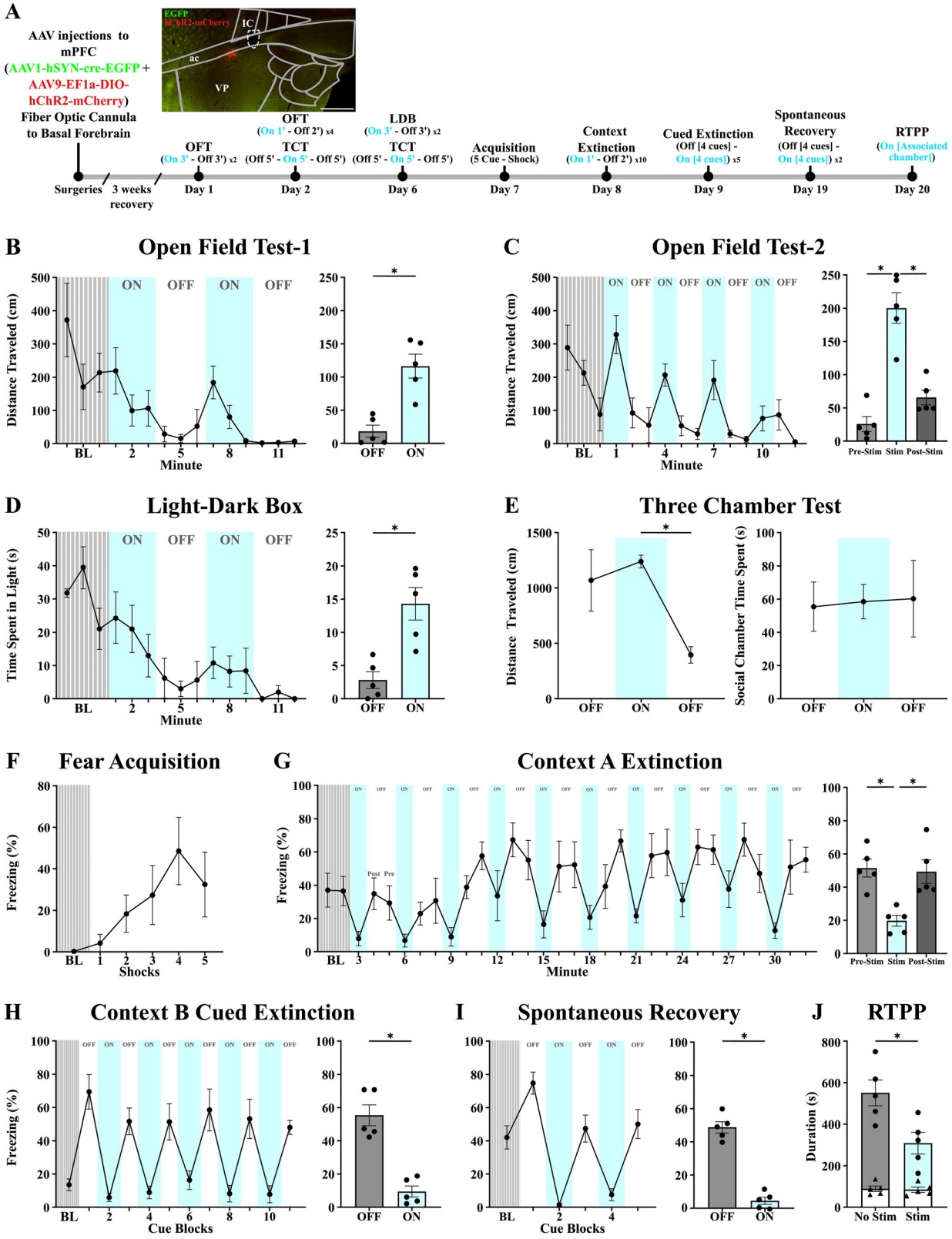

Figure 3. Behavioral effects of optogenetic activation of mPFC–BF projections. ***A***, Experimental timeline and optic cannula locations. EGFP indicates AAV1-hSyn-Cre-EGFP expression, mCherry indicates hChR2-mCherry expression, and the dashed line marks the optic cannula tract (scale bar, 500 µm). ***B***, ***C***, Distance traveled in OFT-1 (***B***) and OFT-2 (***C***) with averaged values across the light ON and OFF epochs in OFT-1 (***B***, right), and across the prestimulation, stimulation, and poststimulation epochs in OFT-2 (***C***, right). ***D***, Time spent in the illuminated chamber during the LDB test with mean values during OFF and ON epochs (right). ***E***, Mean distance traveled during in the TCT (left) with mean time spent in the social zone during (right). ***F***, The percentage of freezing during the acquisition phase of FC. ***G***, The percentage of freezing during context extinction with the average freezing responses during stimulation epochs (right). ***H***, The percentage of freezing during cued extinction with the average freezing responses during OFF and ON epochs (right). ***I***, The percentage of freezing during spontaneous recovery with the average freezing responses during OFF and ON epochs (right). ***J***, Total time spent in the RTPP chamber shown in gray (no stimulation) and blue (stimulation). White inset bars with triangles indicate locomotion time. Error bars represent SEM. $*p < 0.05$.

stimulation (ON) compared with both prestimulation ($p = 0.0002$; 95% CI [−239.4, −109.5]) and poststimulation ($p = 0.0009$; 95% CI [69.7, 199.6]). Activity levels during pre- and poststimulation periods were comparable ($p = 0.245$).

Rearing behavior was higher during stimulation compared with both prestimulation ($p = 0.0005$; 95% CI [−5.84, −2.26]) and poststimulation ($p = 0.0016$; 95% CI [1.61, 5.19]), while pre- and poststimulation epochs did not differ ($p = 0.576$; $F_{(2,8)} = 24.08$; $p = 0.0004$; $\eta^2 = 0.86$). Time spent in the center of the open field showed no effect of stimulation ($t_{(4)} = 2.457$; $p = 0.0699$; 95% CI [−0.36, 6.05]; $\eta^2 = 0.6015$, paired t test).

LDB

Time spent in the light compartment of the LDB across ON–OFF epochs showed a substantial change with stimulation ($F_{(14,56)} = 5.343$; $p < 0.0001$; $\eta^2 = 0.5719$, one-way repeated–measures ANOVA; Fig. 3*D*, left). When averaged across epochs, animals spent significantly more time in the light compartment during ON periods compared with OFF periods ($t_{(4)} = 6.049$; $p = 0.0038$; 95% CI [6.22, 16.78]; $\eta^2 = 0.90$, paired t test; Fig. 3*D*, right). Analysis of light-compartment entries revealed that animals also made significantly more entries into the light compartment during stimulation periods ($t_{(4)} = 4.491$; $p = 0.0109$; 95% CI [0.1400, 0.5934]; $\eta^2 = 0.8345$, paired t test).

TCT

Optogenetic stimulation significantly altered locomotor activity in the TCT ($F_{(2,8)} = 10.96$; $p = 0.0051$; $\eta^2 = 0.7326$, one-way repeated–measures ANOVA; Fig. 3*E*, left). Animals traveled greater distances during the ON period compared with the second OFF period ($p = 0.0055$; 95% CI [298.7, 1,387]), whereas no difference was detected between the ON period and the initial OFF period ($p = 0.6613$). Animals also traveled greater distances during the first OFF period compared with the second OFF period ($p = 0.0187$; 95% CI [129.2, 1,218]). Optogenetic stimulation, however, did not produce significant effects on social preference measures as the time spent in the social chamber containing the conspecific did not differ across conditions ($F_{(2,8)} = 0.0286$; $p = 0.9719$; $\eta^2 = 0.0070$, one-way repeated–measures ANOVA; Fig. 3*E*, right), nor did the duration spent in the social interaction zone surrounding the model animal ($F_{(2,8)} = 1.998$; $p = 0.1977$; $\eta^2 = 0.3332$).

FC

Freezing during cue presentations in the acquisition phase showed a progressive increase across trials, indicating successful fear learning ($F_{(5,20)} = 3.608$; $p = 0.0173$; $\eta^2 = 0.4742$, one-way repeated–measures ANOVA; Fig. 3*F*).

During the context extinction session, we observed a marked reduction in freezing during optogenetic stimulation compared with OFF periods ($F_{(31,124)} = 3.993$; $p < 0.0001$; $\eta^2 = 0.4995$; Fig. 3*G*, left). To further assess this effect, we averaged freezing levels across prestimulation, stimulation, and poststimulation epochs and found a significant main effect of stimulation ($F_{(2,8)} = 33.18$; $p = 0.0001$; $\eta^2 = 0.8924$; Fig. 3*G*, right). Freezing responses of the animals were significantly reduced during ON periods compared with prestimulation ($p = 0.0002$; 95% CI [19.31, 44.22]) and poststimulation epochs ($p = 0.0004$; 95% CI [−42.06, −17.15]), which did not differ from each other ($p = 0.8755$).

In the cued extinction session, freezing behavior during cue presentations was analyzed across blocks of four cues. Freezing decreased during the stimulation blocks but stayed elevated during the no-stimulation blocks. This pattern indicates that the reduction in freezing was driven by the stimulation itself rather than by extinction learning. Consistently, comparing ON and OFF cue periods confirmed a significant reduction in freezing during stimulation ($t_{(4)} = 6.345$; $p = 0.0032$; 95% CI [−66.00, −25.82]; $\eta^2 = 0.91$, paired t test; Fig. 3*H*). Freezing was also reduced during the ITIs ($t_{(4)} = 4.812$; $p = 0.0086$; 95% CI [−43.88, −11.77]; $\eta^2 = 0.85$, paired t test), suggesting that the suppressive effect of stimulation extends beyond cue presentations.

Spontaneous recovery of the conditioned response was evaluated across five consecutive cue blocks, showing a significant change in freezing levels across time ($F_{(5,20)} = 17.46$; $p < 0.000$;, $\eta^2 = 0.81$, one-way repeated–measures ANOVA; Fig. 3*I*, left). Optogenetic stimulation suppressed freezing even after 10 d following cue extinction ($t_{(4)} = 9.636$; $p = 0.0006$; 95% CI [−56.95, −31.47]; $\eta^2 = 0.9587$, paired t test; Fig. 3*I*, right).

RTPP

Animals spent significantly less time in the stimulation-paired compartment compared with the nonstimulation side in the RTPP task, indicating an avoidance response to the optogenetic stimulation of BF-projecting mPFC neurons ($t_{(4)} = 3.080$; $p = 0.0369$; 95% CI [−461.4, −23.95]; $\eta^2 = 0.70$, paired t test; Fig. 3*J*). Locomotor activity was comparable across the two compartments, showing that animals moved similarly on both sides and they had no prior preference toward any of the compartments ($t_{(4)} = 1.435$; $p = 0.2247$; 95% CI [−15.26, 4.86]; $\eta^2 = 0.33$; Fig. 3*J*, white inset bars).

Optogenetic activation of the PrL and IL projections to the BF

For all behavioral measures in the projection-specific experiments, sex was included as a between-subject factor in the corresponding ANOVAs. These analyses revealed no significant main effects of sex and no significant interactions between sex and the relevant within-subject factors for any dependent variable (all $p > 0.05$). Accordingly, data were collapsed across sex for subsequent analyses.

OFT

The IL activation group showed a significant increase in locomotion from the prestimulation to the stimulation/light ON epoch ($p = 0.0089$; 95% CI [−197.0, −21.52]), whereas no-stimulation effects were detected in the PrL ($p = 0.8775$) or control groups ($p = 0.8564$). The control group, however, exhibited significantly higher locomotion during the baseline epoch relative to both subsequent stimulation-free and stimulation periods (Baseline vs Prstimulation, $p = 0.0011$; 95% CI [68.18, 270.8]; Baseline vs Poststimulation, $p = 0.0002$; 95% CI [68.18, 270.8]; Baseline vs Stimulation, $p = 0.0120$; 95% CI [20.77, 223.4]), reflecting their elevated activity at the start of the OFT (Fig. 4*B*, left).

General activity levels varied across stimulation epochs ($F_{(3,60)} = 20.83$; $p < 0.0001$; $\eta^2 = 0.2509$, two-way repeated–measures ANOVA; Fig. 4*B*, right). Similar to the locomotion, increase in general activity is only found in the IL group during optogenetic simulation (Prestimulation vs Stimulation, $p < 0.0001$; 95% CI [−28.28, −8.00]; Stimulation vs Poststimulation, $p = 0.0157$; 95% CI [1.71, 21.99]).

Rearing behavior also differed between stimulation epochs ($F_{(3,60)} = 7.207$; $p = 0.0003$; $\eta^2 = 0.1323$, two-way repeated–measures ANOVA). In the IL activation group, rearing frequency increased from prestimulation to light ON periods ($p < 0.0001$; 95% CI [−5.53, −1.60]). Rearing during the ON period was also

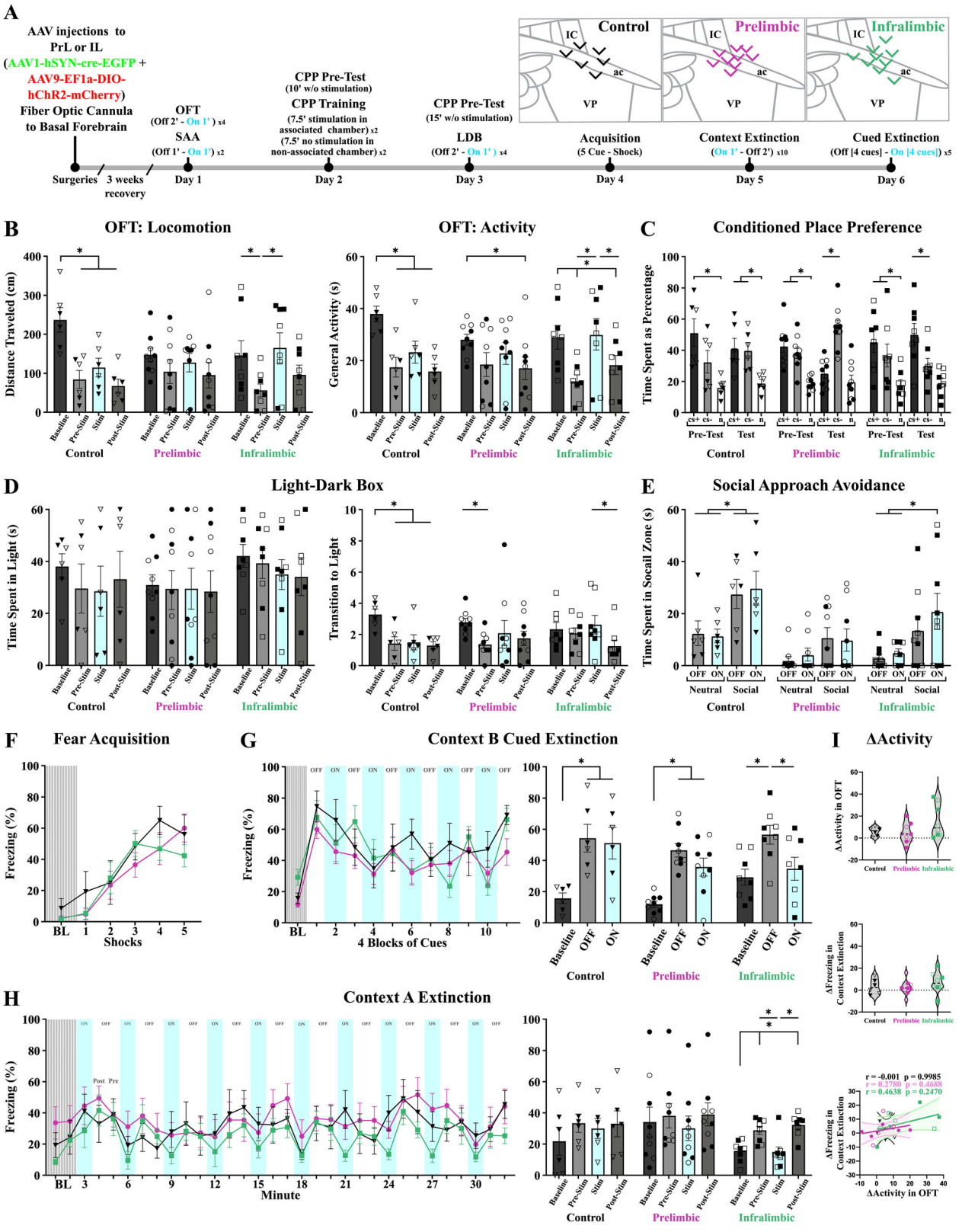

Figure 4. Behavioral effects of optogenetic activation of PrL and IL projections to the BF. ***A***, Experimental timeline and optic cannula locations. ***B***, Distance traveled (left) and general activity levels (right) in OFT. ***C***, The percentage of total time spent in the stimulation associated, no-stimulation associated, and neutral chambers in CPP. ***D***, Time spent in the illuminated chamber during the LDB test (left) with frequency of transition to light compartment (right). ***E***, Time spent in the social zone during the SAA test. ***F***, The percentage of freezing during the acquisition phase of FC. ***G***, The percentage of freezing during cued extinction with the average freezing responses during baseline, OFF, and ON epochs (right). ***H***, The percentage of freezing during context extinction with the average freezing responses during baseline and different stimulation epochs (right). ***I***, Analysis of general activity from prestimulation to stimulation epochs in the OFT and contextual fear extinction. Top, Change in general activity during the OFT. Middle, Change in freezing during context extinction. Bottom, Correlation between change in activity and freezing in the OFT and context extinction. Data points represent individual animals; filled symbols indicate males, and open symbols indicate females. Error bars indicate SEM. $*p < 0.05$.

higher than in the poststimulation period ($p = 0.0034$; 95% CI [0.72, 4.65]), indicating a stimulation-specific transient elevation in rearing.

Time spent in the center of the open field differed across stimulation periods ($F_{(3,60)} = 13.39$; $p < 0.0001$; $\eta^2 = 0.1983$, two-way repeated–measures ANOVA), with no significant group effect ($F_{(2,20)} = 0.70$; $p = 0.5051$) or interaction ($F_{(6,60)} = 1.68$; $p = 0.01409$). IL activation animals spent significantly more time in the center during the baseline epoch compared with the prestimulation ($p < 0.0001$; 95% CI [5.60, 15.97]), stimulation ($p < 0.0001$; 95% CI [4.06, 14.44]), and poststimulation periods ($p < 0.0001$; 95% CI [4.42, 14.80]). In the PrL activation group, animals spent more time in the center of the maze during baseline compared with poststimulation epoch ($p = 0.0307$; 95% CI [0.36, 10.14]).

CPP

The PrL activation group showed an avoidance toward stimulus-associated chamber in the CPP test session following two rounds of conditioning ($p < 0.0001$; 95% CI [−43.85, −14.83]). In contrast, IL activation animals spent more time in the stimulus-paired chamber than the nonassociated zone ($p < 0.0084$; 95% CI [4.39, 35.18]; Fig. 4*C*). The control group showed no differences between the CS^+ and CS^- chambers (all $p > 0.05$). One animal from the IL group lost its cannula implantation during CPP conditioning and was removed from subsequent experiments.

LDB

Optogenetic stimulations did not change the overall time spent in the light compartment ($F_{(3,60)} = 1.92$; $p = 0.1353$; $\eta^2 = 0.014$, two-way repeated–measures ANOVA; Fig. 4*D*, left) but altered the transition frequency to the light compartment ($F_{(3,60)} = 9.06$; $p < 0.0001$; $\eta^2 = 0.1451$; Fig. 4*D*, right). The higher number of transitions was observed in the baseline compared with all periods in the control animals (Baseline vs Prestimulation, $p = 0.0069$; 95% CI [0.40, 3.32]; Baseline vs Stimulation, $p = 0.0108$; 95% CI [0.32, 3.24]; Baseline vs Poststimulation, $p = 0.0035$; 95% CI [0.52, 3.44]). In the IL group, transitions were significantly reduced during the poststimulation period relative to the light ON period ($p = 0.0276$; 95% CI [0.11, 2.64]), whereas the PrL group showed a significant decrease in transitions from baseline to the prestimulation epoch ($p = 0.0134$; 95% CI [0.23, 2.60]).

SAA

Social interaction levels changed significantly during the SAA test session ($F_{(3,63)} = 15.22$; $p < 0.0001$; $\eta^2 = 0.20$, two-way repeated–measures ANOVA; Fig. 4*E*). Control animals spent more time in the interaction zone when a social stimulus (i.e., conspecific) was introduced regardless of optogenetic stimulation (Empty OFF vs Full OFF, $p = 0.0240$; 95% CI [−28.76, −1.48]; Empty ON vs Full ON, $p = 0.0039$; 95% CI [−15.87, 11.41]). Animals in the IL group spent more time in the interaction zone when the social stimulus was present during optogenetic stimulation (ON) compared with both ON and OFF periods when there was no social stimulus (Empty OFF vs Full ON, $p = 0.0004$; 95% CI [−29.03, −6.76]; Empty ON vs Full ON, $p = 0.0020$; 95% CI [−27.02, 3.83]).

Rearing frequency within the social zone also changed across time ($F_{(3,63)} = 6.51$; $p = 0.0007$; $\eta^2 = 0.09$, two-way repeated–measures ANOVA) and differed among groups ($F_{(2,21)} = 7.318$; $p = 0.0039$; $\eta^2 = 0.24$). In the control group, rearing was significantly higher when a social stimulus was present compared with when it was absent (Empty ON vs Full OFF, $p = 0.0461$; 95% CI [−3.75, −0.02]). While the PrL group showed no differences (all $p > 0.05$), rearing was significantly enhanced in the IL group when the social stimulus was presented during optogenetic stimulation (Full ON) compared with optogenetic stimulation alone (Empty ON; $p = 0.0052$; 95% CI [−3.52, −0.48]). This suggests that IL activation enhances social stimulus-evoked rearing rather than driving rearing independently in the SAA test.

FC

Freezing levels increased across shocks during the acquisition phase, indicating successful fear learning ($F_{(5,100)} = 21.91$; $p < 0.0001$; $\eta^2 = 0.44$, two-way repeated–measures ANOVA; Fig. 4*F*). There was no difference between groups ($F_{(2,20)} = 1.13$; $p = 0.3417$; $\eta^2 = 0.01$) indicating that groups exhibited a comparable learning rate.

During context extinction, freezing behavior declined over time ($F_{(31,620)} = 2.91$; $p < 0.0001$; $\eta^2 = 0.07$, two-way repeated–measures ANOVA; Fig. 4*H*, left), with no significant effect of the group ($F_{(2,20)} = 0.93$; $p = 0.4123$; $\eta^2 = 0.033$) or interaction ($F_{(62,620)} = 0.66$; $p = 0.9801$; $\eta^2 = 0.03$). Averaging across stimulation epochs confirmed a main effect of stimulation ($F_{(3,60)} = 8.89$; $p < 0.0001$; $\eta^2 = 0.06$, two-way repeated–measures ANOVA; Fig. 4*H*, right). There was no difference in freezing levels in both control and PrL groups across stimulation epochs. Importantly, in the IL group, stimulation significantly reduced freezing levels compared with both the prestimulation ($p = 0.0126$; 95% CI [2.34, 25.98]) and poststimulation periods ($p = 0.0012$; 95% CI [−29.43, −5.79]), indicating a selective suppression of freezing in this group.

In the cued extinction session, freezing levels varied significantly across cue blocks ($F_{(11,220)} = 9.88$; $p < 0.0001$; $\eta^2 = 0.20$, two-way repeated–measures ANOVA; Fig. 4*G*, left), with no group effect ($F_{(2,20)} = 0.79$; $p = 0.4684$; $\eta^2 = 0.02$) or interaction ($F_{(22,220)} = 1.37$; $p < 0.1317$; $\eta^2 = 0.06$). Visual inspection of the line graph, however, reveals a distinct pattern in the IL group: freezing dropped sharply during stimulation blocks and increased again during nonstimulation blocks, producing oscillations aligned with optogenetic stimulation. When all ON and OFF periods were averaged, we revealed a significant main effect of stimulation on freezing ($F_{(2,40)} = 43.53$; $p < 0.0001$; $\eta^2 = 0.40$, two-way repeated–measures ANOVA; Fig. 4*G*, right). Freezing was significantly higher during OFF periods compared with baseline in all groups (Control, $p < 0.0001$; 95% CI [−55.63, −1.48]; PrL, $p < 0.0001$; 95% CI [−48.51, −20.62]; IL, $p = 0.0002$; 95% CI [−42.08, −12.50]). Importantly, in the IL group, freezing during stimulation was significantly lower than during OFF periods ($p = 0.0025$; 95% CI [7.04, 36.62]), indicating that optogenetic activation reduced freezing to baseline levels observed in the absence of conditioned cues or shocks. This pattern suggests a suppression of fear expression that is specific to stimulation.

Normalized behavioral test comparisons

To address the possibility that baseline differences between groups contributed to the observed effects, we performed additional baseline-normalized analyses (Fig. S1). For OFT and LDB measures, stimulation and poststimulation values were expressed as percentages of baseline values, whereas freezing measures were expressed as changes from baseline.

In the IL group, normalized locomotion significantly increased during stimulation relative to both the prestimulation ($p = 0.003$; 95% CI [−155.4, −43.06]) and poststimulation epochs ($p = 0.0484$; 95% CI [0.3334, 112.6]; Fig. S1*A*). Similarly, normalized

general activity levels varied across stimulation epochs ($F_{(2,40)} = 11.76$; $p < 0.0001$; $\eta^2 = 0.1017$, two-way repeated–measures ANOVA; Fig. S1*B*). Increased activity during optogenetic stimulation was observed only in the IL group (Prestimulation vs Stimulation, $p < 0.0001$; 95% CI [−91.93, −34.99]; Stimulation vs Poststimulation, $p = 0.0041$; 95% CI [11.48, 68.42]).

In the baseline-normalized LDB analysis, time spent in the light compartment did not vary across stimulation epochs ($F_{(2,40)} = 0.2181$; $p = 0.8067$; $\eta^2 = 0.0008$, two-way repeated–measures ANOVA; Fig. S1*C*). In contrast, transitions to the light compartment varied across stimulation epochs ($F_{(2,40)} = 3.94$; $p = 0.0273$; $\eta^2 = 0.05744$; two-way repeated–measures ANOVA; Fig. S1*D*). In the IL group, the number of transitions to the light compartment was lower during the poststimulation epoch than during both the prestimulation ($p = 0.0467$; 95% CI [0.4826, 79.84]) and stimulation periods ($p = 0.0006$; 95% CI [26.73, 106.1]; Fig. S1*D*).

When freezing was expressed as change from baseline, the overall pattern remained unchanged (Fig. S1*E*,*F*). During cued extinction, freezing levels differed between ON and OFF epochs ($F_{(1,20)} = 17.78$; $p = 0.0004$; $\eta^2 = 0.0805$, two-way repeated–measures ANOVA; Fig. S1*E*). Reduced freezing during ON epochs was observed only in the IL group ($p = 0.0005$; 95% CI [9.53, 34.13]). Similarly, in the baseline-normalized context extinction analysis, freezing levels varied across stimulation epochs ($F_{(2,40)} = 19.17$; $p < 0.0001$; $\eta^2 = 0.0701$, two-way repeated–measures ANOVA; Fig. S1*F*). In the IL group, freezing during stimulation was reduced relative to both the prestimulation ($p = 0.0089$; 95% CI [4.41, 23.91]) and poststimulation epochs ($p = 0.0034$; 95% CI [−27.76, −7.47]).

Together, the baseline-normalized analyses indicate that the primary effects observed in the original analyses remained significant after controlling for baseline differences, suggesting that the reported stimulation-related behavioral effects were not driven by prestimulation variability between groups.

Relationship between locomotor activity and conditioned freezing

We compared general activity in the OFT with freezing levels in FC to assess whether acquired fear responses are affected by differential activity levels among groups. For this purpose, Δ-scores were computed separately for general activity levels in the OFT and freezing reduction during the context extinction session. For the OFT, Δ-activity was defined as stimulation to prestimulation activity, whereas in context extinction Δ-freezing was defined as prestimulation to stimulation freezing, so that positive values consistently reflect increased activity or reduced freezing.

There was no difference between groups on Δ-activity ($F_{(2,20)} = 2.485$; $p = 0.1087$; $\eta^2 = 0.20$; Fig. 4*I*, top). Although the overall effect was nonsignificant, data suggested that IL animals showed a tendency toward higher Δ-activity compared with controls animals. For Δ-freezing reduction, the group effect was likewise nonsignificant ($F_{(2,20)} = 0.8334$; $p = 0.4491$; $\eta^2 = 0.007$; Fig. 4*I*, middle).

Pearson's correlations were calculated for each group in order to test whether stimulation-induced changes in general activity were related to changes in freezing. In the PrL group, Δ-activity showed a weak positive association with Δ-freezing reduction ($r = 0.28$; 95% CI [–0.47, 0.79]; $p = 0.4688$). In the IL group, Δ-activity showed a moderate positive association with Δ-freezing reduction ($r = 0.46$; 95% CI [–0.36, 0.88]; $p = 0.2470$; Fig. 4*I*, bottom). No meaningful correlations were observed in the control group ($r \approx 0$; $p = 0.9985$).

Together, these results indicate that IL stimulation can promote activity, as reflected by increases in Δ-activity. Importantly, the IL group exhibited the largest reduction in freezing, suggesting that lower freezing levels may partially reflect enhanced general activity during optogenetic stimulation.

Molecular profile of BF-targeting mPFC neurons

The molecular composition of mPFC neurons projecting to the BF was examined by assessing the expression of parvalbumin (PV), calbindin (CB), CaMKIIa, and mDlx in retrogradely labeled neurons in the PrL and IL cortices (Fig. 5). Following dual virus injections, very few BF-projecting neurons in either the PrL or IL regions expressed mDlx (Fig. 5*B*). In another pair of animals, AAV9-CaMKIIa-hM4D(Gi)-mCherry injections into the mPFC labeled CaMKIIa-expressing neurons predominantly in deep cortical layers, whereas most BF-projecting neurons in the PrL and IL are located in Layers 3 and 5 (Fig. 5*A*). This may have possibly resulted in an underrepresentation of CaMKIIa-expressing BF–projecting mPFC neurons (Fig. 5*C*).

PV and CB were analyzed in eight animals using up to three coronal mPFC sections per animal, yielding 37 and 36 data points, respectively. CaMKIIa was analyzed in seven animals using up to four sections per animal, yielding 48 data points. mDlx-based viral labeling was analyzed in a separate cohort of two animals, using up to three sections per animal, yielding 11 data points. Immunohistochemical analysis revealed that ∼5% of BF-targeting neurons in both the PrL and IL were PV-immunopositive (Fig. 5*D*), while a relatively larger proportion of neurons were CB-immunopositive (Fig. 5*E*). Based on all viral expression and immunohistochemical analyses (Fig. 5*F–U*), no significant differences were observed between PrL- and IL-projecting populations for any of the molecular markers (paired *t* tests, all $p > 0.05$).

Postsynaptic targets in the ventral pallidum

We examined the postsynaptic targets of the densest mPFC projections to the BF arising from the IL. In these animals, optic cannula placement in the BF overlapped with dense IL-derived axonal projections, confirming effective targeting of prefrontal terminals within BF subregions, primarily the ventral pallidum (Fig. 6*A*). High power confocal imaging revealed that IL axons labeled with mCherry formed dense arborizations within the VP and closely apposed neurons identified through anterograde transsynaptic labeling as well as immunohistochemistry.

To characterize the putative synaptic contacts, we performed immunohistochemistry for postsynaptic density protein 95 (PSD95), vesicular glutamate transporter 2 (VGluT2), and gephyrin. IL axons in the VP were frequently observed in very close apposition to PSD95-positive postsynaptic puncta, consistent with excitatory synaptic specializations at sites of axonal contact (Fig. 6*B–D*). Some of these terminal-like axonal profiles also exhibited VGluT2 immunoreactivity across BF subregions, further supporting a potential glutamatergic nature (Fig. 6*E–G*). In contrast, gephyrin immunoreactivity, a marker of inhibitory postsynaptic specializations, did not show clear overlap in the sections examined (Fig. 6*H–J*). Notably, multiple gephyrin-positive puncta were present within the VP, confirming successful labeling.

The postsynaptic targets of IL axons in the VP were identified by combining anterograde transsynaptic viral tracing with fluorescent immunohistochemistry (Fig. 6*K–O*). Injection of AAV1-hSyn-Cre-EGFP into the mPFC resulted in robust labeling of postsynaptic neurons in the ventral pallidum and to a

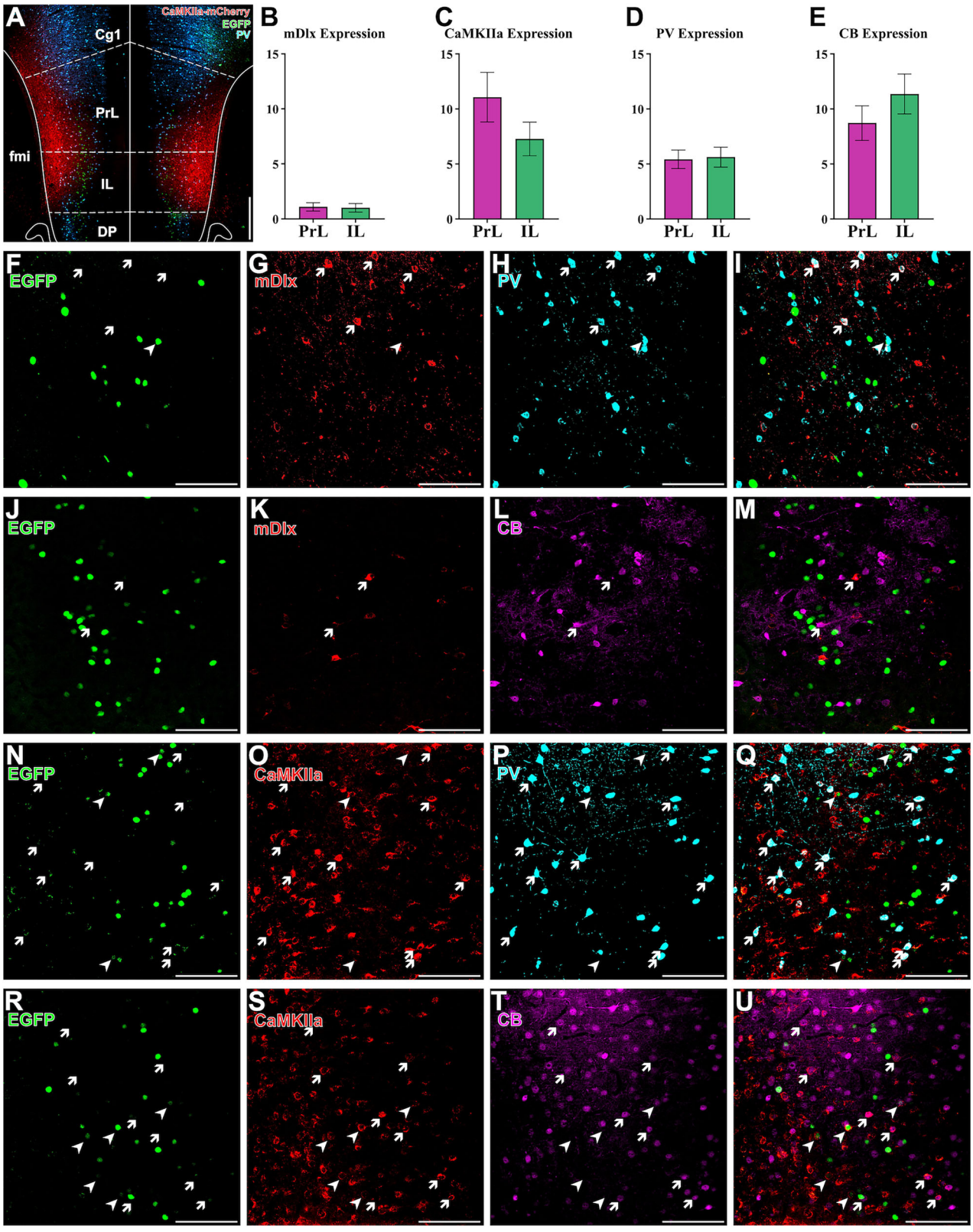

Figure 5. Molecular characterization of BF-projecting mPFC neurons. ***A***, Low-magnification confocal image showing viral expression and immunohistochemical labeling in the mPFC (scale bar, 500 µm). ***B–E***, The percentage of retrogradely labeled neurons expressing mDlx (***B***), CaMKIIa (***C***), PV (***D***), and CB (***E***) in the PrL and IL cortices. ***F, J, N, R***, Retrogradely labeled neurons in the mPFC following AAVretro-hSyn-Cre-EGFP injections into the BF. ***G, K, O, S***, mDlx- or CaMKIIa-expressing neurons following AAV9-CaMKIIa-hM4D(Gi)-mCherry or AAV9-mDlx-ChR2-mCherry-Fishell-3 injections into the mPFC. ***H, L, P, T***, PV- or CB-immunopositive neurons. ***I, M, Q, U***, Overlay images showing triple channel colocalization. Arrows indicate mCherry-expressing cells overlapping with PV^+ or CB^+ neurons. Arrowheads indicate overlaps between retrogradely labeled EGFP cells and $mCherry^+$, PV^+, or CB^+ neurons (scale bars, 100 µm).

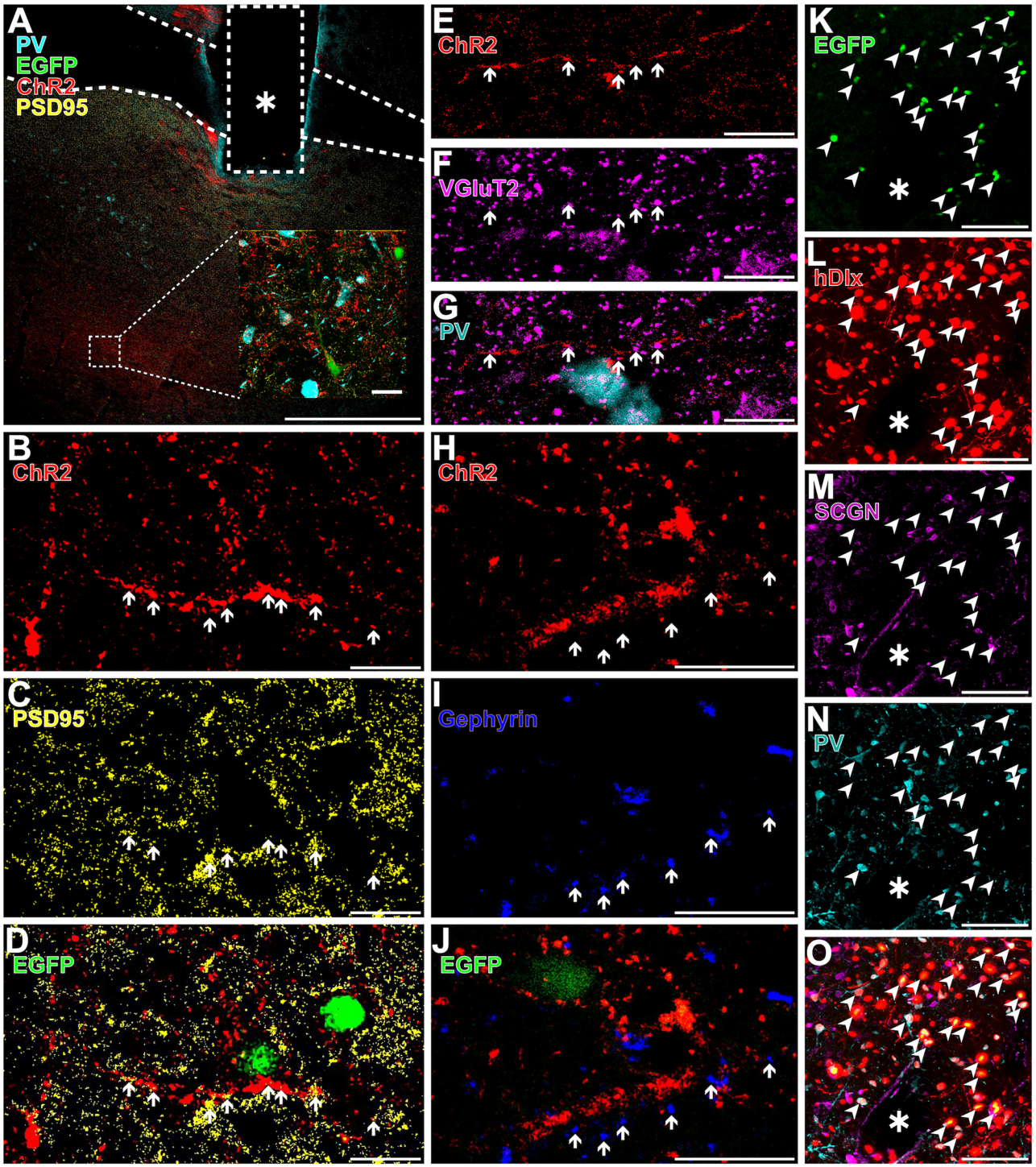

Figure 6. Confocal microscopic characterization of postsynaptic targets of the IL neurons in the VP. ***A***, Representative low-magnification image from the IL–BF optogenetic activation experiment showing dense IL axonal profiles (arrows) within the VP and the placement of the optic cannula (asterisk; scale bar, 500 µm). ***B–D***, IL-derived axons (mCherry, red) form dense arborizations within the ventral pallidum and closely appose neurons labeled through anterograde transsynaptic tracing (EGFP). PSD95 immunoreactivity is observed in close proximity to axonal profiles. ***E–G***, VGluT2 immunoreactivity along axonal profiles apposed to a PV-immunopositive neuron. ***H–J***, Gephyrin-positive puncta are present in the BF tissue but do not overlap with axonal terminals (scale bars in ***B–J***, 25 µm). ***K–O***, Anterograde transsynaptic labeling of BF neurons from the IL (***K***) and hDlx-driven reporter expression (***L***) with immunohistochemistry for SCGN (***M***) and PV (***N***), showing colocalization between transsynaptically labeled neurons (arrowheads) and inhibitory neuronal subtypes in the BF. Asterisks mark the cannula implantation site (***A***) or the viral injection sites (***K–O***). Scale bars, 100 µm.

lesser extent in the substantia innominata and the horizontal diagonal band. Subsequent injection of AAV9-hDlx-GiDREADD-dTomato-Fishell5 into the BF selectively labeled inhibitory neurons. Observed overlap between the EGFP and dTomato signals revealed BF inhibitory neurons receiving mPFC input, confirming direct connectivity between mPFC axons and inhibitory VP populations, particularly in the ventral pallidum. Among these postsynaptic neurons, secretagogin (SCGN) expression was comparatively sparse (Fig. 6*M*,*O*), whereas a substantial subset expressed PV (Fig. 6*N*,*O*).

We further characterized the postsynaptic targets of prefrontal neurons within the VP using a dual-viral approach. Injection of AAV1-hSyn-Cre-EGFP into the mPFC enabled dense anterograde transsynaptic labeling of downstream target neurons. In parallel, cell type-specific viral vectors driven by distinct promoters were injected into the VP to label putative GABAergic, cholinergic, or CaMKIIa$^+$ populations, allowing assessment of their overlap with mPFC-recipient neurons. Leu-enkephalin immunohistochemistry was used to delineate the borders of the VP (Haber and Nauta, 1983; Heimer et al., 1991), confirming that mPFC-recipient neurons were located within the leu-enkephalin-rich VP (Fig. 7*A–I*). hDlx-labeled putative GABAergic neurons were abundant throughout the region and also extended into surrounding areas (Fig. 7*B*). Cholinergic neurons were distributed across the VP, with a relatively higher density in the lateral VP (Fig. 7*E*). In contrast, CaMKIIa-labeled neurons were mostly localized to the ventrolateral VP (Fig. 7*H*).

For overlap quantification, five sections were analyzed per animal, yielding a total of 10 sections per group. The ChAT, hDlx, and CaMKIIα groups consisted of separate cohorts of animals, with each group used to assess overlap between mPFC-recipient neurons and a specific VP neuronal population. In all cases, both mPFC and VP injection sites were verified, and sections were excluded if injections were off-target or viral expression was insufficient, resulting in 15 data points per group included in the final analysis. Quantification revealed that the majority of mPFC-recipient neurons (Fig. 7*J*,*N*,*R*) overlapped with hDlx-labeled (Fig. 7*K*,*L*) putative GABAergic neurons (88.28 ± 2.94%; mean ± SEM; $n = 15$; Fig. 7*M*), whereas substantially lower overlap was observed with ChAT-labeled (Fig. 7*O*,*P*) cholinergic neurons (17.50 ± 2.22%; $n = 15$; Fig. 7*Q*) and CaMKIIa-labeled (Fig. 7*S*,*T*) neurons (9.65 ± 2.07%; $n = 15$; Fig. 7*U*). Together, these findings indicate that mPFC projections within the VP preferentially target GABAergic neurons.

Discussion

We demonstrated that BF-targeting mPFC neurons are strongly recruited by both acute and chronic stress. Optogenetic activation of these neurons increased locomotor activity, reduced conditioned freezing, and was associated with place avoidance. We then tested the specific contributions of PrL and IL projections to the BF, which primarily target the ventral pallidum. IL, but not PrL, innervation robustly increased general activity and species-specific exploratory behaviors and reduced freezing to baseline levels during cued and contextual fear extinction. Stimulation of the IL–BF pathway was associated with positive valence, as reflected by increased preference for the stimulation-paired chamber in the CPP test. In contrast, PrL–BF pathway activation produced avoidance toward the stimulation-paired chamber without altering activity levels. Anatomical observations revealed that IL projections to the BF were substantially denser than PrL–BF projections. Upstream neurons in both pathways express CaMKIIa and CB, giving rise to VGluT2$^+$ excitatory axonal profiles that appose putative GABAergic neurons in the VP and colocalize with PSD95-positive postsynaptic puncta.

Stress-induced c-Fos mapping revealed substantial neuronal activity in the mPFC, with greater activation following acute stress than chronic stress. We included both CRS and CVS to determine whether recruitment of mPFC neurons depends on the specific form of chronic stress exposure, but no differences were observed between these conditions. Together, these findings suggest that BF-projecting mPFC neurons are recruited across multiple stress paradigms, with greater sensitivity to acute stress exposure.

The rapid increase in activity following mPFC–BF stimulation suggests a role in behavioral activation (Nieh et al., 2016; Salamone et al., 2017), consistent with the idea that stimulation of select BF and hypothalamic circuits may "embolden" behavior (Reichard et al., 2019). The BF regulates motivational state through its effects on cortical arousal and limbic processing (Mogenson et al., 1980; Anaclet et al., 2015; Hangya et al., 2015; Maness et al., 2022), and specific BF circuits promote transitions toward active behavioral states and exploratory engagement (Johnson et al., 2016; Stephenson-Jones et al., 2020). The mPFC modulates BF functioning via direct projections originating from both PrL and IL subregions (Vertes, 2004; Gabbott et al., 2005). Affective regulatory signals originating from the mPFC may bias BF output toward behavioral activation across contexts, as many mPFC–BF neurons were consistently recruited by different forms of stress. Accordingly, increased activity was observed not only in the OFT but also in anxiety-related tasks such as the LDB and TCT, as well as during fear extinction. These effects were selectively driven by IL efferents, as IL–BF, but not PrL–BF, activation reproduced these patterns and promoted active over passive behaviors.

The suppression of conditioned freezing observed following IL–BF activation during both context and cued extinction sessions implicates this pathway in the regulation of fear memory and extinction learning (Quirk and Mueller, 2008; Do-Monte et al., 2015). Early studies demonstrated that activity in the IL cortex suppresses conditioned fear and supports extinction, whereas PrL activity promotes the expression of conditioned fear (Milad and Quirk, 2002; Vidal-Gonzalez et al., 2006). Subsequent work further showed that IL neuronal firing decreases during freezing and increases during extinction learning (Do-Monte et al., 2015; Giustino and Maren, 2015), and, importantly, IL projections to the VP are activated during extinction learning to constrain the freezing response (Fernandes-Henriques et al., 2025). These findings should be considered alongside the established role of IL signaling to the basolateral amygdala in extinction learning (Quirk and Mueller, 2008). Recent work suggests that IL projections to the VP and basolateral amygdala may contribute to partially distinct phases of extinction (Fernandes-Henriques et al., 2025). Our observations extend these findings by showing that heightened IL output may engage BF circuitry to promote behavioral activation across contexts, both under stress-free conditions and during strong conditioned fear.

The VP receives the majority of mPFC projections targeting the BF (Golmayo et al., 2003) and plays a central role in assigning motivational value to stimuli (Stephenson-Jones et al., 2020; Vento and Jhou, 2020; Faget et al., 2024; Kim et al., 2024; Oh et al., 2025). It is therefore well positioned to integrate cortical signals related to motivational context and stimulus value. Consistent with this framework, our pathway-specific manipulations revealed opposing effects of PrL and IL projections in CPP. IL–BF activation produced a positive valence, with animals preferring the stimulation-paired context, whereas PrL–BF activation induced aversion, similar to overall mPFC–BF stimulation. These findings indicate that IL and PrL projections to the BF may differentially assign valence to neutral stimuli, biasing behavior toward approach or avoidance. Accordingly, IL–BF stimulation may promote positive motivation-related BF activity, facilitating exploratory and approach-related behaviors across multiple behavioral contexts.

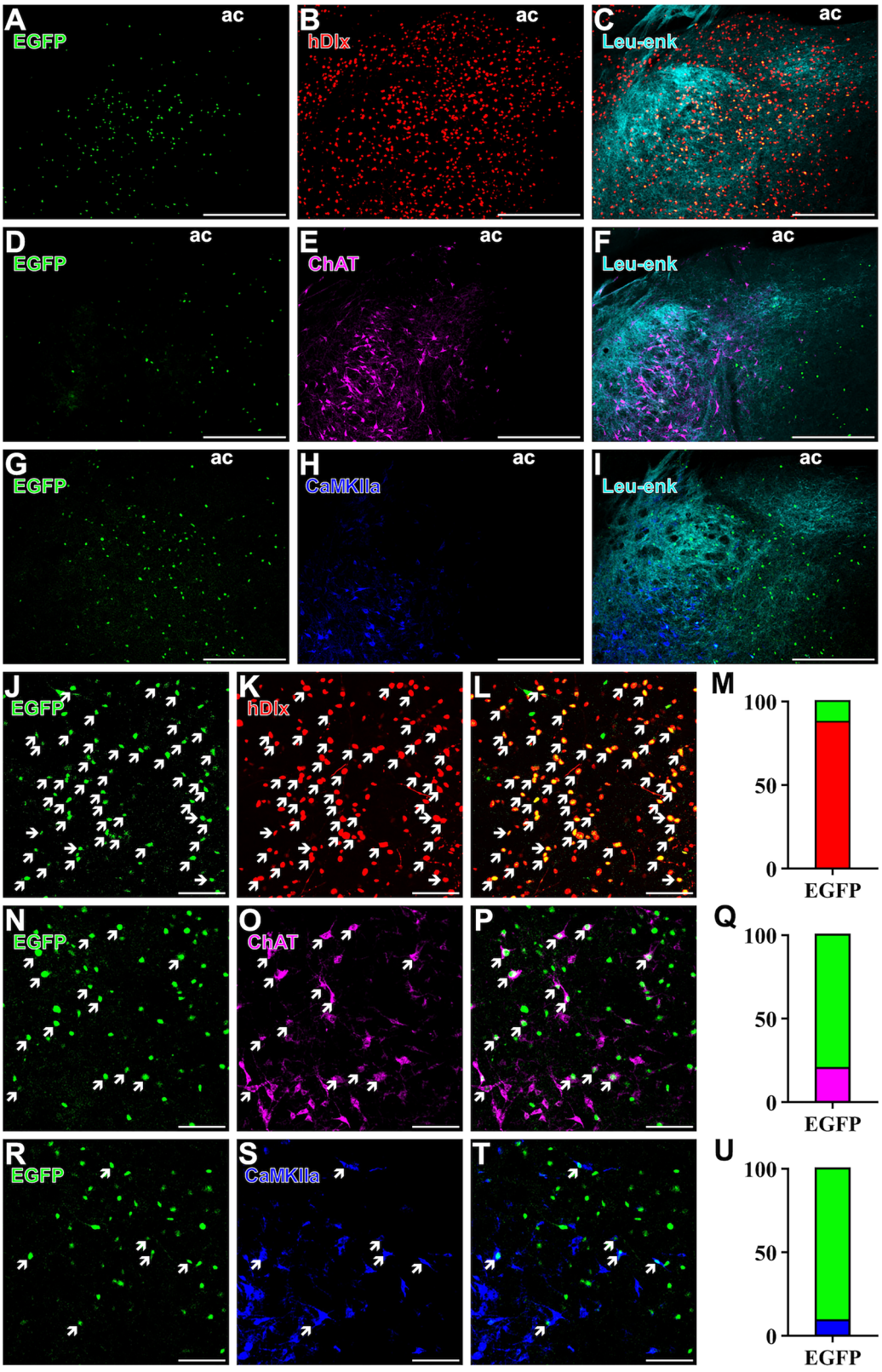

Figure 7. Characterization and quantification of postsynaptic targets of mPFC neurons in the VP. ***A–I***, Representative low-magnification images showing the distribution of mPFC-recipient neurons labeled by EGFP following anterograde transsynaptic labeling (***A***, ***D***, ***G***) in relation to putative GABAergic (hDlx; ***B***), cholinergic (ChAT; ***E***), and CaMKIIa^{+} (***H***) neuronal populations; overlaid with leu-enkephalin (Leu-enk) labeling to delineate the borders of the VP (***C***, ***F***, ***I***). Scale bars, 500 µm. ***J–U***, Confocal images showing EGFP-labeled mPFC-recipient neurons coexpressing hDlx (***J–L***), ChAT (***N–P***), or CaMKIIa (***R–T***) in the VP (arrows; scale bars, 50 µm), together with quantification of the percentage of mPFC-recipient neurons colocalizing with hDlx (***M***), ChAT (***Q***), or CaMKIIa (***U***) populations.

This dissociation in valence encoding aligns with evidence that IL and PrL cortices differentially regulate affective processing via distinct downstream projections. In mPFC–amygdala pathways, IL activity is associated with safety and extinction signaling, whereas PrL engagement promotes threat evaluation and aversive responding (Burgos-Robles et al., 2013; Likhtik et al., 2014; Do-Monte et al., 2015). Similarly, PrL and ventral striatum activity correlates with avoidance behavior (Bravo-Rivera et al., 2015), while IL–nucleus accumbens activation is self-rewarding (Cameron et al., 2019). Opposing effects of IL and PrL outputs have also been reported in projections to neuromodulatory centers (Watanabe et al., 2025). Here, PrL–BF activation abolished the natural preference for social interaction, whereas IL–BF activation preserved social bias during light ON periods. Likewise, IL–BF stimulation induced CPP, while PrL–BF stimulation caused avoidance. Together, these findings indicate that PrL and IL inputs to the BF differentially encode valence and guide context-appropriate behavior.

The behavioral effects of IL–BF activation observed in some tests are difficult to dissociate into purely locomotor or affective components, as these dimensions are often expressed together at the level of behavioral output (Vinck et al., 2015; Lu et al., 2020). In this context, the reduction in freezing and increase in activity produced by IL–BF stimulation may reflect a broader shift in behavioral state rather than a selective effect on a single process. This issue is particularly relevant for the extinction experiments, where freezing levels are likely influenced by both increased activity and memory processes (Quirk and Mueller, 2008). In contrast, the CPP induced by IL–BF stimulation, together with the avoidance produced by PrL–BF stimulation, strongly supports a valence-related component beyond activity increase, as CPP is widely used to infer the rewarding or aversive value of an experience from subsequent chamber preference (Prus et al., 2009). Moreover, because optogenetic stimulation was limited to the conditioning sessions and absent during the pretest and test phases, the chamber bias observed at test is unlikely to reflect stimulation-associated locomotor effects and more likely reflects the valence of the stimulation-paired compartment.

Molecular characterization of BF-projecting mPFC neurons revealed that only a minority of retrogradely labeled neurons expressed the markers examined. This limited overlap likely reflects both population heterogeneity and methodological constraints related to viral access. Although CaMKIIa expression is reported across most cortical layers of the rodent mPFC (Yao et al., 2023), our CaMKIIa-driven viral expression was biased toward deeper layers. In contrast, BF-projecting neurons were mainly located in middle layers, likely reducing labeling efficiency. Thus, more BF-projecting neurons may express CaMKIIa than detected here. In addition, the limited expression of PV, CB, and mDlx in subsets of PrL and IL neurons suggests that BF-projecting mPFC neurons are more heterogeneous than previously thought.

IL–BF projections were denser than PrL projections and reached the BF predominantly via the internal capsule, consistent with prior studies (Vertes, 2004). Both subregions primarily targeted the VP, with hDlx-expressing putative GABAergic neurons comprising the principal target population. A subset of these neurons coexpressed various calcium-binding proteins. Some of the axonal profiles, both en passant and terminal, were clearly immunopositive for VGluT2 or closely apposed to PSD95-positive postsynaptic puncta, consistent with a glutamatergic identity. In contrast, we did not observe colocalization of mPFC axons with gephyrin, a scaffolding protein marking inhibitory postsynaptic sites. Together, these findings suggest that mPFC provides excitatory drive to GABAergic neurons in the VP.

Distinct VP neuronal populations differentially regulate approach-avoidance behavior, with glutamatergic neurons promoting threat avoidance and GABAergic neurons supporting reward-seeking while suppressing stress-related motor activity (Stephenson-Jones et al., 2020; Faget et al., 2024). In our experiments, IL–BF activation sustained social interaction, suggesting recruitment of GABAergic VP neurons involved in social reward-seeking, whereas PrL–BF activation abolished this effect. Notably, IL, but not PrL, projections promoted active threat avoidance, suggesting that IL projections may target a distinct subset of GABAergic neurons functionally separate from the broader VP GABAergic population.

In conclusion, this study demonstrates that distinct forms of stress recruit BF-projecting mPFC neurons that give rise to two pathways with opposing, or complimentary, functions. These effects emerge from a molecularly heterogeneous population of glutamatergic mPFC neurons that preferentially engage inhibitory VP neurons. Together, these findings identify the BF as a key node in prefrontal control of affective function, through which PrL and IL efferents differentially regulate motivational state, valence processing, and extinction learning. In line with broader principles of subregion-specific prefrontal control, IL–BF projections bias behavior toward active and approach-related states, whereas the PrL–BF pathway favors avoidance.

References

Adhikari A, et al. (2015) Basomedial amygdala mediates top-down control of anxiety and fear. Nature 527:179–185.

Akirav I, Maroun M (2007) The role of the medial prefrontal cortex-amygdala circuit in stress effects on the extinction of fear. Neural Plast 2007:30873.

Akmese C, Sevinc C, Halim S, Unal G (2023) Differential role of GABAergic and cholinergic ventral pallidal neurons in behavioral despair, conditioned fear memory and active coping. Prog Neuropsychopharmacol Biol Psychiatry 125:110760.

Anaclet C, Pedersen NP, Ferrari LL, Venner A, Bass CE, Arrigoni E, Fuller PM (2015) Basal forebrain control of wakefulness and cortical rhythms. Nat Commun 6:8744.

Bloodgood DW, Sugam JA, Holmes A, Kash TL (2018) Fear extinction requires infralimbic cortex projections to the basolateral amygdala. Transl Psychiatry 8:60.

Bravo-Rivera C, Roman-Ortiz C, Montesinos-Cartagena M, Quirk GJ (2015) Persistent active avoidance correlates with activity in prelimbic cortex and ventral striatum. Front Behav Neurosci 9:184.

Burgos-Robles A, Bravo-Rivera H, Quirk GJ (2013) Prelimbic and infralimbic neurons signal distinct aspects of appetitive instrumental behavior. PLoS One 8:e57575.

Cameron CM, Murugan M, Choi JY, Engel EA, Witten IB (2019) Increased cocaine motivation is associated with degraded spatial and temporal representations in IL-NAc neurons. Neuron 103:80–91.e7.

Corcoran KA, Quirk GJ (2007) Activity in prelimbic cortex is necessary for the expression of learned, but not innate, fears. J Neurosci 27:840–844.

de Kloet SF, Bruinsma B, Terra H, Heistek TS, Passchier EMJ, van den Berg AR, Luchicchi A, Min R, Pattij T, Mansvelder HD (2021) Bi-directional regulation of cognitive control by distinct prefrontal cortical output neurons to thalamus and striatum. Nat Commun 12:1994.

Dimidschstein J, et al. (2016) A viral strategy for targeting and manipulating interneurons across vertebrate species. Nat Neurosci 19:1743–1749.

Dixon ML, Thiruchselvam R, Todd R, Christoff K (2017) Emotion and the prefrontal cortex: an integrative review. Psychol Bull 143:1033–1081.

Do-Monte FH, Manzano-Nieves G, Quiñones-Laracuente K, Ramos-Medina L, Quirk GJ (2015) Revisiting the role of infralimbic cortex in fear extinction with optogenetics. J Neurosci 35:3607–3615.

Faget L, Oriol L, Lee W-C, Zell V, Sargent C, Flores A, Hollon NG, Ramanathan D, Hnasko TS (2024) Ventral pallidum GABA and

glutamate neurons drive approach and avoidance through distinct modulation of VTA cell types. Nat Commun 15:4233.
Fernandes-Henriques C, Guetta Y, Sclar MG, Zhang R, Miura Y, Surrence KR, Friedman AK, Likhtik E (2025) Infralimbic projections to the substantia innominata–ventral pallidum constrain defensive behavior during extinction learning. J Neurosci 45:e1001242025.
Furlanis E, et al. (2025) An enhancer-AAV toolbox to target and manipulate distinct interneuron subtypes. Neuron 113:1525–1547.e15.
Gabbott PLA, Warner TA, Jays PRL, Bacon SJ (2003) Areal and synaptic interconnectivity of prelimbic (area 32), infralimbic (area 25) and insular cortices in the rat. Brain Res 993:59–71.
Gabbott PLA, Warner TA, Jays PRL, Salway P, Busby SJ (2005) Prefrontal cortex in the rat: projections to subcortical autonomic, motor, and limbic centers. J Comp Neurol 492:145–177.
Gaykema RP, van Weeghel R, Hersh LB, Luiten PG (1991) Prefrontal cortical projections to the cholinergic neurons in the basal forebrain. J Comp Neurol 303:563–583.
Gencturk S, Unal G (2024) Rodent tests of depression and anxiety: construct validity and translational relevance. Cogn Affect Behav Neurosci 24:191–224.
Gielow MR, Zaborszky L (2017) The input-output relationship of the cholinergic basal forebrain. Cell Rep 18:1817–1830.
Giustino TF, Maren S (2015) The role of the medial prefrontal cortex in the conditioning and extinction of fear. Front Behav Neurosci 9:298.
Giustino TF, Fitzgerald PJ, Maren S (2016) Fear expression suppresses medial prefrontal cortical firing in rats. PLoS One 11:e0165256.
Golmayo L, Nuñez A, Zaborszky L (2003) Electrophysiological evidence for the existence of a posterior cortical-prefrontal-basal forebrain circuitry in modulating sensory responses in visual and somatosensory rat cortical areas. Neuroscience 119:597–609.
Gyengési E, Zaborszky L, Détári L (2008) The effect of prefrontal stimulation on the firing of basal forebrain neurons in urethane anesthetized rat. Brain Res Bull 75:570–580.
Haber SN, Nauta WJ (1983) Ramifications of the globus pallidus in the rat as indicated by patterns of immunohistochemistry. Neuroscience 9:245–260.
Hangya B, Ranade SP, Lorenc M, Kepecs A (2015) Central cholinergic neurons are rapidly recruited by reinforcement feedback. Cell 162:1155–1168.
Hänsel A, von Känel R (2008) The ventro-medial prefrontal cortex: a major link between the autonomic nervous system, regulation of emotion, and stress reactivity? Biopsychosoc Med 2:21.
Hartley CA, Phelps EA (2010) Changing fear: the neurocircuitry of emotion regulation. Neuropsychopharmacology 35:136–146.
Hegedüs P, Király B, Schlingloff D, Lyakhova V, Velencei A, Szabó Í, Mayer MI, Zelenak Z, Nyiri G, Hangya B (2024) Parvalbumin-expressing basal forebrain neurons mediate learning from negative experience. Nat Commun 15:4768.
Heimer L, Zahm DS, Churchill L, Kalivas PW, Wohltmann C (1991) Specificity in the projection patterns of accumbal core and shell in the rat. Neuroscience 41:89–125.
Hurley KM, Herbert H, Moga MM, Saper CB (1991) Efferent projections of the infralimbic cortex of the rat. J Comp Neurol 308:249–276.
Johnson SB, Emmons EB, Anderson RM, Glanz RM, Romig-Martin SA, Narayanan NS, LaLumiere RT, Radley JJ (2016) A basal forebrain site coordinates the modulation of endocrine and behavioral stress responses via divergent neural pathways. J Neurosci 36:8687–8699.
Johnson SB, Lingg RT, Skog TD, Hinz DC, Romig-Martin SA, Viau V, Narayanan NS, Radley JJ (2022) Activity in a prefrontal-periaqueductal gray circuit overcomes behavioral and endocrine features of the passive coping stress response. Proc Natl Acad Sci U S A 119:e2210783119.
Kenwood MM, Kalin NH, Barbas H (2022) The prefrontal cortex, pathological anxiety, and anxiety disorders. Neuropsychopharmacology 47:260–275.
Kim R, Ananth MR, Desai NS, Role LW, Talmage DA (2024) Distinct subpopulations of ventral pallidal cholinergic projection neurons encode valence of olfactory stimuli. Cell Rep 43:114009.
Kingir E, Sevinc C, Unal G (2023) Chronic oral ketamine prevents anhedonia and alters neuronal activation in the lateral habenula and nucleus accumbens in rats under chronic unpredictable mild stress. Neuropharmacology 228:109468.
Kitanishi T, Tashiro M, Kitanishi N, Mizuseki K (2022) Intersectional, anterograde transsynaptic targeting of neurons receiving monosynaptic inputs from two upstream regions. Commun Biol 5:149.
Leung C, Kim JC, Jia Z (2018) Three-chamber social approach task with optogenetic stimulation (mice). Bio Protoc 8:e3120.
Likhtik E, Stujenske JM, Topiwala MA, Harris AZ, Gordon JA (2014) Prefrontal entrainment of amygdala activity signals safety in learned fear and innate anxiety. Nat Neurosci 17:106–113.
Lu L, et al. (2020) Control of locomotor speed, arousal, and hippocampal theta rhythms by the nucleus incertus. Nat Commun 11:262.
Maness EB, Burk JA, McKenna JT, Schiffino FL, Strecker RE, McCoy JG (2022) Role of the locus coeruleus and basal forebrain in arousal and attention. Brain Res Bull 188:47–58.
McKlveen JM, Myers B, Herman JP (2015) The medial prefrontal cortex: coordinator of autonomic, neuroendocrine and behavioural responses to stress. J Neuroendocrinol 27:446–456.
Milad MR, Quirk GJ (2002) Neurons in medial prefrontal cortex signal memory for fear extinction. Nature 420:70–74.
Moaddab M, Ray MH, McDannald MA (2021) Ventral pallidum neurons dynamically signal relative threat. Commun Biol 4:43.
Mogenson GJ, Jones DL, Yim CY (1980) From motivation to action: functional interface between the limbic system and the motor system. Prog Neurobiol 14:69–97.
Moorman DE, Aston-Jones G (2015) Prefrontal neurons encode context-based response execution and inhibition in reward seeking and extinction. Proc Natl Acad Sci U S A 112:9472–9477.
Nett KE, Zimbelman AR, McGregor MS, Alizo Vera V, Harris MR, LaLumiere RT (2023) Infralimbic projections to the nucleus accumbens shell and amygdala regulate the encoding of cocaine extinction learning. J Neurosci 43:1348–1359.
Nieh EH, et al. (2016) Inhibitory input from the lateral hypothalamus to the ventral tegmental area disinhibits dopamine neurons and promotes behavioral activation article inhibitory input from the lateral hypothalamus to the ventral tegmental area disinhibits dopamine neurons. Neuron 90: 1286–1298.
Oh J-MN, Amemori S, Takada M, Amemori K-I (2025) Differential representation of motivation and affective judgment by neurons in the primate ventral striatum and ventral pallidum during approach-avoidance decision-making. Neurosci Res 219:104955.
Paxinos G, Watson C (2006) *The rat brain in stereotaxic coordinates: hard cover*. Amsterdam: Access Online via Elsevier.
Pennington ZT, Dong Z, Feng Y, Vetere LM, Page-Harley L, Shuman T, Cai DJ (2019) Eztrack: an open-source video analysis pipeline for the investigation of animal behavior. Sci Rep 9:19979.
Prus AJ, James JR, Rosecrans JA (2009) *Conditioned Place Preference*. (J. J. Buccafusco, Ed.).
Quirk GJ, Mueller D (2008) Neural mechanisms of extinction learning and retrieval. Neuropsychopharmacology 33:56–72.
Reichard RA, Parsley KP, Subramanian S, Stevenson HS, Schwartz ZM, Sura T, Zahm DS (2019) The lateral preoptic area and ventral pallidum embolden behavior. Brain Struct Funct 224:1245–1265.
Rizzo V, et al. (2017) Encoding of contextual fear memory requires de novo proteins in the prelimbic cortex. Biol Psychiatry Cogn Neurosci Neuroimaging 2:158–169.
Room P, Russchen FT, Groenewegen HJ, Lohman AH (1985) Efferent connections of the prelimbic (area 32) and the infralimbic (area 25) cortices: an anterograde tracing study in the cat. J Comp Neurol 242:40–55.
Salamone J, Correa M, Yohn S, Yang J-H, Somerville M, Rotolo R, Presby R (2017) Behavioral activation, effort-based choice, and elasticity of demand for motivational stimuli: basic and translational neuroscience approaches. Motiv Sci 3:208–229.
Schindelin J, et al. (2012) Fiji: an open-source platform for biological-image analysis. Nat Methods 9:676–682.
Shih C-W, Chang C-H (2024) Anatomical analyses of collateral prefrontal cortex projections to the basolateral amygdala and the nucleus accumbens core in rats. Brain Struct Funct 229:97–114.
Sierra-Mercado D, Padilla-Coreano N, Quirk GJ (2011) Dissociable roles of prelimbic and infralimbic cortices, ventral hippocampus, and basolateral amygdala in the expression and extinction of conditioned fear. Neuropsychopharmacology 36:529–538.
Sotres-Bayon F, Quirk GJ (2010) Prefrontal control of fear: more than just extinction. Curr Opin Neurobiol 20:231–235.
Stephenson-Jones M, Bravo-Rivera C, Ahrens S, Furlan A, Xiao X, Fernandes-Henriques C, Li B (2020) Opposing contributions of GABAergic and glutamatergic ventral pallidal neurons to motivational behaviors. Neuron 105:921–933.e5.

Stringer C, Wang T, Michaelos M, Pachitariu M (2021) Cellpose: a generalist algorithm for cellular segmentation. Nat Methods 18:100–106.
Tao Y, Cai C-Y, Xian J-Y, Kou X-L, Lin Y-H, Qin C, Wu H-Y, Chang L, Luo C-X, Zhu D-Y (2021) Projections from infralimbic cortex to paraventricular thalamus mediate fear extinction retrieval. Neurosci Bull 37:229–241.
Totty MS, Tuna T, Ramanathan KR, Jin J, Peters SE, Maren S (2023) Thalamic nucleus reuniens coordinates prefrontal-hippocampal synchrony to suppress extinguished fear. Nat Commun 14:6565.
Vento PJ, Jhou TC (2020) Bidirectional valence encoding in the ventral pallidum. Neuron 105:766–768.
Vertes RP (2004) Differential projections of the infralimbic and prelimbic cortex in the rat. Synapse 51:32–58.
Vidal-Gonzalez I, Vidal-Gonzalez B, Rauch SL, Quirk GJ (2006) Microstimulation reveals opposing influences of prelimbic and infralimbic cortex on the expression of conditioned fear. Learn Mem 13:728–733.
Vinck M, Batista-Brito R, Knoblich U, Cardin JA (2015) Arousal and locomotion make distinct contributions to cortical activity patterns and visual encoding. Neuron 86:740–754.
Watanabe M, Uematsu A, Johansen JP (2025) Bidirectional emotional regulation through prefrontal innervation of the locus coeruleus. Mol Psychiatry 30:3568–3578.
Woon EP, Sequeira MK, Barbee BR, Gourley SL (2020) Involvement of the rodent prelimbic and medial orbitofrontal cortices in goal-directed action: a brief review. J Neurosci Res 98:1020–1030.
Yao Z, et al. (2023) A high-resolution transcriptomic and spatial atlas of cell types in the whole mouse brain. Nature 624:317–332.
Zaborszky L (2002) The modular organization of brain systems. Basal forebrain: the last frontier. Prog Brain Res 136:359–372.
Zaborszky L, Gaykema RP, Swanson DJ, Cullinan WE (1997) Cortical input to the basal forebrain. Neuroscience 79:1051–1078.